PEEK Titanium Composite (PTC) for Spinal Implants

Erik I. Waldorff, Samuel Fang, Nianli Zhang, Livia Visai, Marcello Imbriani, Emanuele Magalini, Eleonora Preve, Pierfrancesco Robotti, Andrew L. Raines, Evan Goldberg, Jiechao Jiang, Kirk C. McGilvray, Jeremiah Easley, Howard B. Seim, Christian M. Puttlitz, and James T. Ryaby

E. I. Waldorff (✉) · S. Fang · N. Zhang · J. T. Ryaby
Orthofix, Inc., Lewisville, TX, USA
e-mail: erikwaldorff@orthofix.com

L. Visai
Department of Molecular Medicine, Center for Health Technologies (CHT),
INSTM UdR of Pavia, University of Pavia, Pavia, Italy

Department of Occupational Medicine, Toxicology and Environmental Risks,
Istituti Clinici Scientifici (ICS) Maugeri, IRCCS, Pavia, Italy

M. Imbriani
Department of Occupational Medicine, Toxicology and Environmental Risks,
Istituti Clinici Scientifici (ICS) Maugeri, IRCCS, Pavia, Italy

Department of Public Health, Experimental Medicine and Forensics, University of Pavia,
Pavia, Italy

E. Magalini · E. Preve · P. Robotti
Eurocoating S.p.A, Trento, Italy

A. L. Raines · E. Goldberg
Translational Testing and Training Laboratories, Inc., T3 Labs, Atlanta, GA, USA

J. Jiang
Department of Material Science, University of Texas at Arlington, Arlington, TX, USA

K. C. McGilvray · C. M. Puttlitz
Orthopaedic Bioengineering Research Laboratory (OBRL), Department of Mechanical
Engineering, Colorado State University, Fort Collins, CO, USA

J. Easley · H. B. Seim
Preclinical Surgical Research Laboratory (PSRL), Colorado State University, Fort Collins, CO, USA

1 Introduction

Since the development of the posterior lumbar interbody fusion (PLIF) and anterior approach for anterior cervical discectomy and fusion (ACDF) [1–4], many different fusion substrates such as grafts and devices have been explored. This includes autografts [5], allografts [6], and interbody spacers made from polyether-ether-ketone (PEEK) [7], porous tantalum [8], and titanium [29]. Autografts used to be the standard due to their high fusion rate, however, disadvantages associated with them include donor site morbidity with potential pain and numbness at the donor site [9, 10]. Allografts do not possess the autograft disadvantage of donor site morbidity, but have been associated with the risk of infection, disease transmission, and issues with histocompatibility [9]. In addition, a meta-analysis for one- and two-level ACDF comparing autografts and allografts showed a statistically superior fusion rate for autografts [6]. However, other studies have found no difference in fusion rates between autografts and allografts for multi-level ACDFs [11]. PEEK devices have been found to be the new gold standard for the treatment of lumbar and cervical disc disease [12, 13], showing similar fusion rates as autografts for PLIF and ACDF [14–16]. Despite possessing the advantages of radiolucency for radiographic determination of fusion, this may simultaneously make dislodgement and subsidence difficult to determine for PEEK devices. Another disadvantage of PEEK is that it is bioinert, which limits incorporation into the fusion mass and the subsequent implant stability [17–19]. Hence, in order to improve on the PEEK device fusion rate, stability, bone apposition and anchoring, new porous devices have been developed such as porous tantalum and titanium [8, 29]. These devices possess similar stiffness as PEEK, which has a stiffness in the range between cancellous and cortical bone [20, 21], thus avoiding stress shielding.

The concept of changing the material, shape and surface of the implants builds on the fact that integration of the implant device with the native tissue is dependent on its interactions with undifferentiated stem cells and osteoblasts [22–27] and is influenced by its surface properties [28]. These surface properties include topography, porosity, chemistry, surface energy, and surface charge [22, 28]. Modifications to optimize the surface properties of implant materials have been performed with the goal of facilitating new bone growth around and within the surgical area and assimilation with the device [22]. In general, the topographical character of roughness of titanium is associated with long-term cell adhesion, and surface topography and chemistry impact proliferation and differentiation [22, 29]. The integration of the substrate material with the biological environment of the surgical area is enhanced by higher porosity and larger pore sizes [30], with data from in vivo titanium models of osteogenesis indicating that pore sizes in the range of 300–400 μm are optimal [30]. Many interbody fusion devices have thus incorporated the concept of porous or roughened metals using various titanium or tantalum alloys (Titan Spine, Mequon, WI; Medtronic, Minneapolis, MN; Zimmer, Inc., Warsaw, IN). By using these alloys in a porous form, the mechanical properties of the devices can approach that of trabecular bone, thus avoiding stress shielding [31]. However, common for all of these devices is the use of the alloy throughout the device. Thus, despite possessing a

superior osteogenic surface to PEEK, interbody devices made from only porous titanium or tantalum are difficult to image, causing artifacts on radiographs, CT images and MRI scans hindering perfect assessment of spinal fusion [32–34]. Both PEEK and titanium fulfill the requirement of biocompatibility in order to prevent host rejection of implants, device failure, and potential costly and painful revision surgeries [26, 35–39]. In an attempt to combine only the advantages from both the PEEK and titanium interbody devices, a novel type of PEEK titanium composite (PTC) interbody fusion device has been developed. This device combines a PEEK core with titanium alloy endplates made from a novel 3-dimensional (3D) titanium mesh to potentially enable a better bone apposition and ingrowth while enabling imaging of the fusion site. The endplates are made of the alloy Ti6Al4V, which has demonstrated osseointegration within 4–8 weeks following implantation in in vivo studies using textured implants composed of titanium foam [37], a titanium alloy Ti6Al4V core with titanium fiber-mesh bonded onto the core [38], or dense versus porous titanium [39]. However, the Ti6Al4V endplates for the PTC device were constructed to have a novel D pattern while using a novel manufacturing method.

This chapter will present how the novel PTC interbody devices are manufactured, which applications the PTC technology have currently been applied to, and how the mechanical properties of the interbody devices that employ the PTC technology compare to that of standard PEEK devices. In addition, the surface topography of the Ti6Al4V endplates will be discussed alongside a presentation of several in vitro and in vivo studies that have been completed for the PTC technology. Specifically, two in vitro studies will be presented showing the effect of each of the structural components (PEEK, Ti6Al4V) on the proliferation and differentiation of immature and mature osteoblasts. Furthermore, two in vivo studies will illustrate the effect of the structural components (PEEK, Ti6Al4V) on bone ingrowth/ongrowth and biocompatibility in a rabbit model, and the effect of a clinical PTC device in an ovine lumbar fusion model. Lastly, a discussion will summarize the presented studies and make the case for the PTC technology as a new standard for interbody devices in spine fusion.

2 Manufacturing and Applications

2.1 Manufacturing

The manufacturing and assembly of the Ti6Al4V endplates for the PTC is novel and performed in the following manner. First, the material (Ti6Al4V) used for the production of the Ti porous raw plate is obtained with the Selective Laser Melting (SLM) method, an Additive Manufacturing (AM) technique, which is based on the concept of creating a 3D designed object by means of consolidation of the material layer by layer until the full part is completed [40]. The SLM process is considered distinct from traditional machining techniques, which mostly rely on the removal of material by methods such as cutting or drilling (subtractive processes). The manufacturing
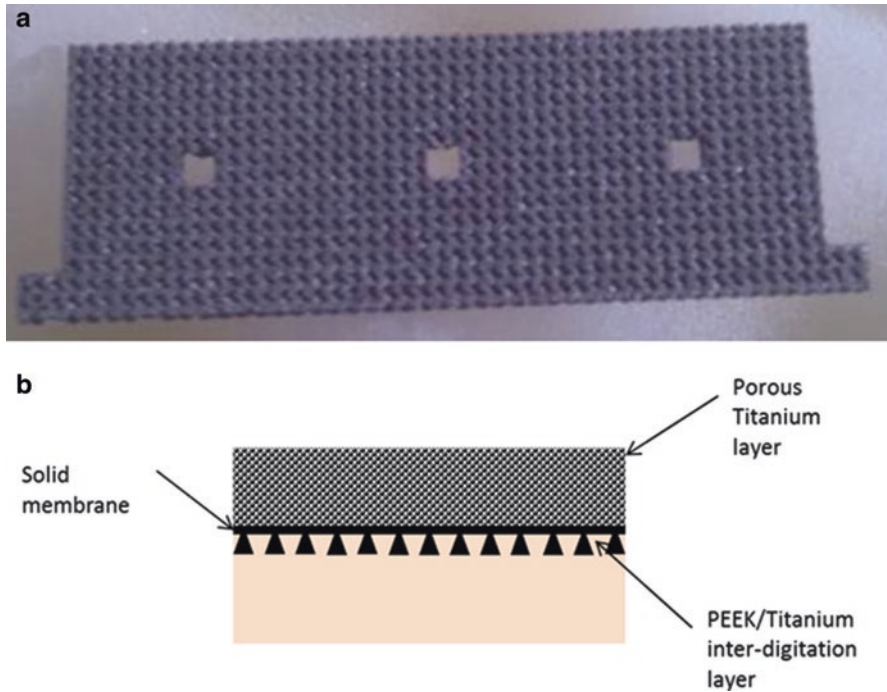
Fig. 1 Manufacturing details of the PTC technology. (**a**) Single Ti6Al4V plate post AM processing and thermal treatment but prior to sectioning for final assembly. (**b**) Illustration of the PTC three-layered sandwich structure

method is based on laser melting of metallic powder (Ti6Al4V). A solid-state laser is used as the energy source and a fine Ti6Al4V powder (spherical gas or plasma atomized powder with a grain size lower than 50 μm) as the raw material. The unique 3D design of the endplate is based on previous investigations into bio-reactivity to various designs [41]. Once the AM process, the subsequent proprietary acid etching process and thermal treatment are complete, the final product is a single plate (Fig. 1a) ready for the final manipulations (sectioning) necessary to obtain the final spinal implant. The final Ti6Al4V plate has a porosity of 50%, 400-μm pore size, and 100% interconnectivity. The chemical and physical material properties of the final plate are in agreement with the standards for Ti6Al4V medical devices [42].

Once the Ti6Al4V plate has been sectioned to fit the PTC device, the PEEK core and the two Ti6Al4V endplates are molded together. To create a secure and consistent bonding between the porous titanium structure and PEEK material, a novel three layered sandwich structure is used (Fig. 1b). The PEEK/titanium inter-digitation layer is a layer that combines the two materials together. At this layer, the titanium has an array of solid dovetail structures. During the injection molding process, molten PEEK flows into the grooves formed between the dove tails. Between these two layers (the porous titanium top layer and the PEEK/titanium inter-digitation layer), there is a thin solid titanium membrane layer that serves as a barrier preventing PEEK overflow into the porous titanium layer during the injection molding process.

After the molding, the PEEK material solidifies and forms a strong mechanical bond between the titanium endplates and the PEEK core.

2.2 PTC Applications

The specific PTC technology incorporating the novel manufacturing of endplates made of porous Ti6Al4V (Sect. 2.1) was developed by Orthofix, Inc. (Lewisville, Texas, USA) and has since been applied to several standard spinal fixation interbody devices available. Specifically, the PTC technology has been applied to a standard lumbar interbody device (FORZA® PTC Spacer System), a standard cervical interbody device (CONSTRUX® Mini PTC Spacer System), and a standalone lumbar interbody device (PILLAR® SA PTC Spacer System). Figure 2 illustrates the visual difference between the PTC devices and their standard PEEK device equivalent.

Similar to the standard PEEK interbody devices (Fig. 2b, d, f), the PTC devices (Fig. 2a, c, e) are also intended to be used with autograft and/or allograft both within the intended hallow core or surrounding the device. In addition, the PTC devices have the same indication as the standard PEEK interbody devices (Table 1).

3 Mechanical Properties

3.1 Methods

3.1.1 Testing Setup

To investigate the comparative strength of a PTC interbody device and its equivalent PEEK device, the CONSTRUX Mini PTC cervical interbody device and the CONSTRUX Mini PEEK device were tested under axial compression, torsion and compression-shear loads in accordance with ASTM standard F2077 (Test methods for intervertebral body fusion devices) [43]. These testing modes are used as an industrial standard to characterize the mechanical performance of interbody devices enabling results between various devices to be compared. In accordance with ASTM F2077, a total of 12 devices (6 CONSTRUX Mini PTC, 6 CONSTRUX Mini PEEK) were tested for each testing mode. The size of the implant was chosen to represent a worst-case scenario, i.e., a scenario where the implant size most prone to failure under loading was chosen. This was done for both CONSTRUX Mini PTC and CONSTRUX Mini PEEK. Based on prior analysis for all testing modes (data not shown) the implant with a foot print of 12 × 12 mm was chosen as the worst case for both implants while the height was 6 mm and 5 mm for the CONSTRUX Mini PTC and CONSTRUX Mini PEEK, respectively, as CONSTRUX Mini PTC has no 5 mm offering. Using a 858 MiniBionix hydraulic testing frame (MTC corporation, Eden Prairie, MN), all tests were performed at room temperature in air per ASTM
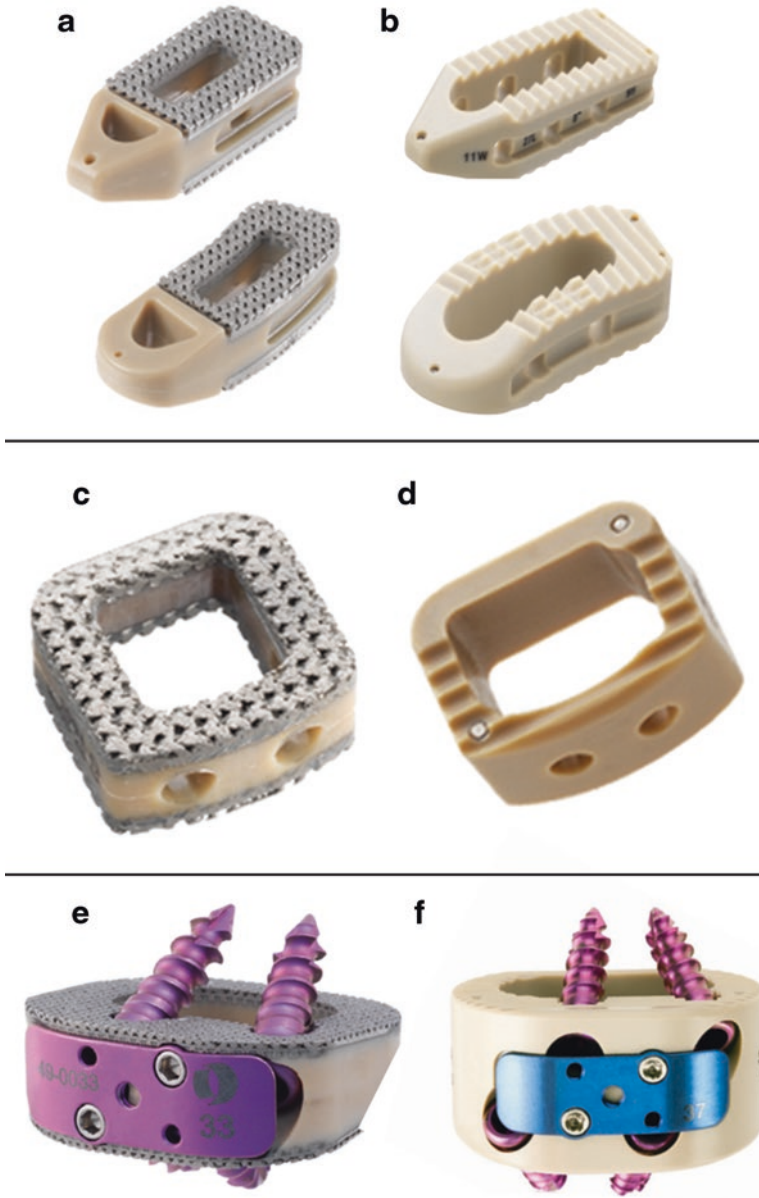
Fig. 2 Current PTC devices using the novel Ti6Al4V endplates and their PEEK equivalents. (**a**) FORZA® PTC Spacer System; lumbar. (**b**) FORZA® PEEK Spacer System; lumbar. (**c**) CONSTRUX® Mini PTC Spacer System; cervical. (**d**) CONSTRUX® Mini PEEK Spacer System; cervical. (**e**) PILLAR® SA PTC Spacer System; lumbar standalone. (**f**) PILLAR® SA PEEK Spacer System; lumbar standalone

Table 1 PTC device type, indication, spine location, levels and year it was approved by the FDA

PTC device	FORZA® PTC Spacer System	CONSTRUX® Mini PTC Spacer System	PILLAR® SA PTC Spacer System
Device type (fixation)	Standard	Standard	Stand alone
Indication	Spinal fusion procedures at one or two contiguous levels in skeletally mature patients with degenerative disc disease (DDD)	Spinal fusion procedures at one or two contiguous levels in skeletally mature patients with DDD	Spinal fusion procedures at one or two contiguous levels in skeletally mature patients with DDD
Spine location	Lumbar	Cervical	Lumbar
Levels	L2-S1	C2-T1	L2-S1
Year approved by the FDA	2015	2012	2016

F2077. The devices were placed between two stainless steel test blocks with pockets matching the outer geometry of the implant (Fig. 3a, b). The pockets provided exact positioning and alignment of the devices to the applied load during testing. Figure 3b shows the cross sectional view of this set up. The depth of the pocket was designed so that the interface between the porous plate and the PEEK was fully exposed to the stress caused by the external loading (Fig. 3b). The test setup was identical between for the two interbody devices.

For axial compression and torsion test, an axial or torsion load was applied to the sample in a displacement-controlled fashion (0.2 mm/s for axial load and 1°/s for torsion load) until device failure. For compression-shear testing, the devices were oriented in a 45-degree anterior-posterior orientation relative to the loading direction. A displacement controlled shear load (0.2 mm/s) was applied until device failure. The yield load (2% strain offset from initial yield per ASTM F2077) was recorded for all tests and normalized to the yield load of the CONSTRUX Mini PEEK device.

3.1.2 Statistical Analysis

The means and standard deviations for the different yield loads were calculated and normalized to the PEEK device for the particular testing method. Statistical differences were determined by unpaired two-tailed t tests with a significance level of $P < 0.05$. Differences between yield loads between the PEEK and PTC devices were assessed.
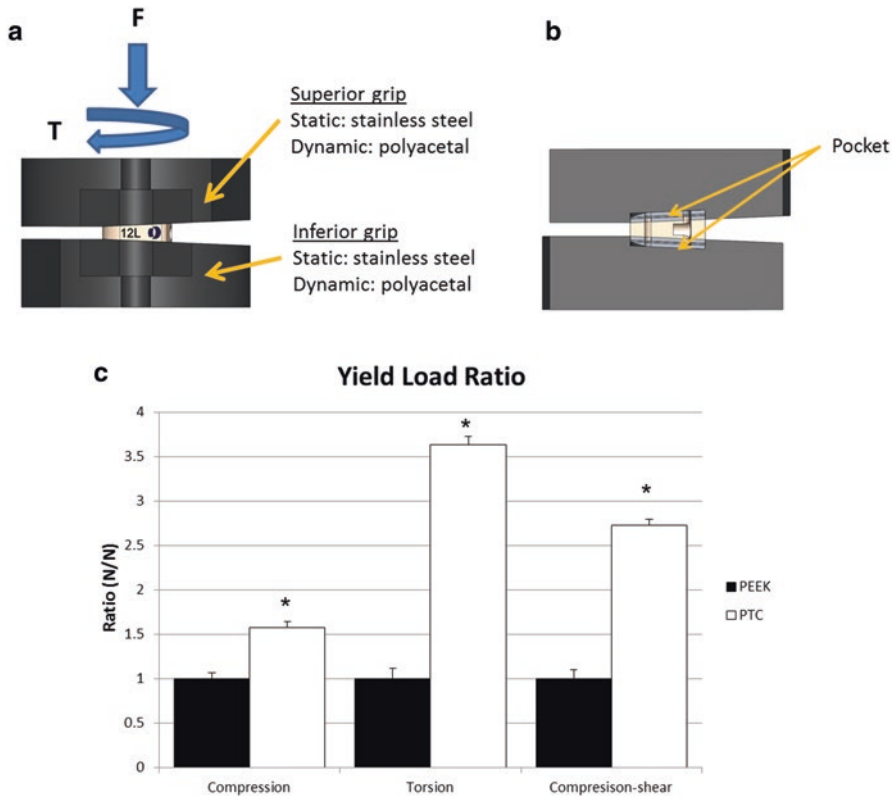
Fig. 3 Mechanical characterization of the CONSTRUX Mini PTC device relative to its PEEK equivalent. (**a**) Mechanical testing grip setup used for compression, torsion loads. Compression-shear loads were achieved by orienting the grip setup in a 45-degrees anterior-posterior orientation relative to the loading direction. (**b**) Cross sectional view of grip setup illustrating device pocket. (**c**) Yield load comparison between CONSTRUX Mini PEEK and CONSTRUX Mini PTC for static compression, torsion and compression-shear tests. Yield loads were normalized to the yield load of the CONSTRUX Mini PEEK device for each test. Statistical significance is indicated for PEEK vs. PTC comparison (*P < 0.05)

3.2   Results

Figure 3C shows the comparison of the normalized yield loads for axial compression, torsion and compression-shear loading conditions between the CONSTRUX Mini PEEK and CONSTRUX Mini PTC devices. Specifically it is seen that the PTC device has a 58%, 264% and 173% higher yield loads than the PEEK device for axial compression, torsion and compression-shear loading, respectively. These differences were all statistically significant.

4 Surface Topographic Characterization

As part of the manufacturing process (Sect. 2.1) the Ti6Al4V endplates also undergo a proprietary acid etching process which generates a micro- and nano-scale surface texture to the individual struts within the porous endplates. Manipulation of the surface at a micro- or nano-scale can alter the Ti6Al4V surface roughness [44] which in turn has been shown to make the local osteogenic environment more favorable [45, 46]. To examine the Ti6Al4V surface topography, the micro-roughness of a typical PTC endplate single strut of the porous titanium plate was examined. In addition, an examination of the PEEK titanium inter-digestion layer was done to investigate the interface between the PEEK core and the Ti6Al4V endplates. Finally, the PTC endplate struts were examined for the presence of nano-scale structures. The information presented on the PTC endplate surface topography examinations has previously been presented in part as an abstract at a scientific conference [47].

4.1 Methods

For the examination, a single PTC interbody spacer was used (FORZA PTC Spacer System). The surface morphology and the micro-roughness of one single strut of the porous Ti6Al4V PTC endplate were investigated using atomic force microscopy (AFM) on a Park XE 70 AFM system using contact mode. AFM measures the sample surface structure using atomic force between the tip and sample via a probe directly interacting with a sample surface. The probe tip is made from SiO_2 mounted onto a cantilever. A probe motion sensor senses the spacing between the tip apex and the sample and provides a correction signal to control the piezoelectric scanner movement. Near-field forces between the tip and sample were detected by a laser beam deflection system. Surface Roughness including (1) Peak to Valley Roughness (Rpv), (2) Root Mean Square Roughness (Rq), (3) Roughness Average (Ra) and (4) Ten Points Roughness Average (Rz) were obtained using an XEI Image Processing Program for SPM data.

The PEEK titanium inter-digestion layer was examined using scanning electron microscopy (SEM) on a Hitachi S-3000N Variable Pressure Scanning Electron Microscope. Secondary electron (SE) imaging was used to characterize the surface morphology of the porous Ti6Al4V structure in a high-vacuum mode. Back scattered electron (BSE) imaging of the PTC implant (side view) was used to study the interface structure between the Ti6Al4V structure and PEEK in a low vacuum mode (30 Pa). An accelerating voltage of 25 kV was used for the SEM studies.

The nanostructure on the surface of one single strut of the porous Ti6Al4V PTC endplate was examined using high-resolution SEM in a Hitachi S-4800 field-emission SEM microscope from the top view direction. For SE imaging, an accelerating voltage of 5 kV and 20 kV were used to characterize the nanostructure.
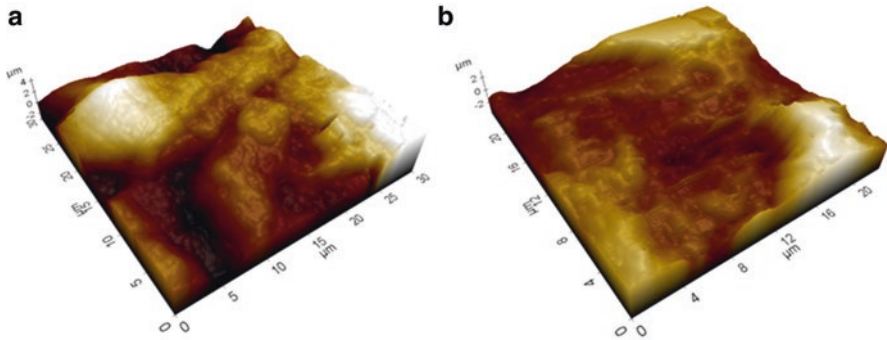
Fig. 4 3D AFM images of Ti6Al4V strut of the PTC device taken from the (**a**) convex and (**b**) concave regions

Table 2 Surface roughness examination of a single strut of the porous Ti6Al4V PTC endplate. Seven locations were examined for Peak to Valley Roughness (Rpv), Root Mean Square Roughness (Rq), Roughness Average (Ra) and Ten Points Roughness Average (Rz)

Area	Rpv (µm)	Rq (µm)	Ra (µm)	Rz (µm)
# 1	7.793	1.194	0.954	7.288
# 2	8.645	1.854	1.427	8.632
# 3	7.012	1.074	0.87	5.884
# 4	9.051	2.39	1.904	9.041
#5	6.952	2.013	1.717	6.937
# 6	8.118	2.35	2.082	8.102
# 7	7.229	1.484	1.179	7.117
Avg.	7.829	1.766	1.448	7.572
St.Dev.	0.821	0.530	0.471	1.088

4.2   Results

Figure 4 presents two typical 3D AFM images taken from two distinct locations showing the morphology of the convex and concave region on the surface of a single strut (Fig. 4a, b, respectively). Seven areas on the surface from the single strut were examined. The micro-roughness measurements over these areas showed that the measured average Peak to Valley Roughness (R_{pv}) is about 7.83 µm, the average Root Mean Square Roughness (R_q) is about 1.77 µm, the Roughness Average (R_a) is about 1.45 µm and the Ten Points Roughness Average (R_z) is 7.57 µm (Table 2).

SEM images of the PTC device from the top view direction obtained at a low magnification (25×) for an overview presented a very well defined structure (Fig. 5a), while the SEM images obtained at a large magnification (3000×) presents a well determined honeycomb like porous structure on the surface (Fig. 5d). SEM images from the side view along both X and Y directions shown in Fig. 5a revealed
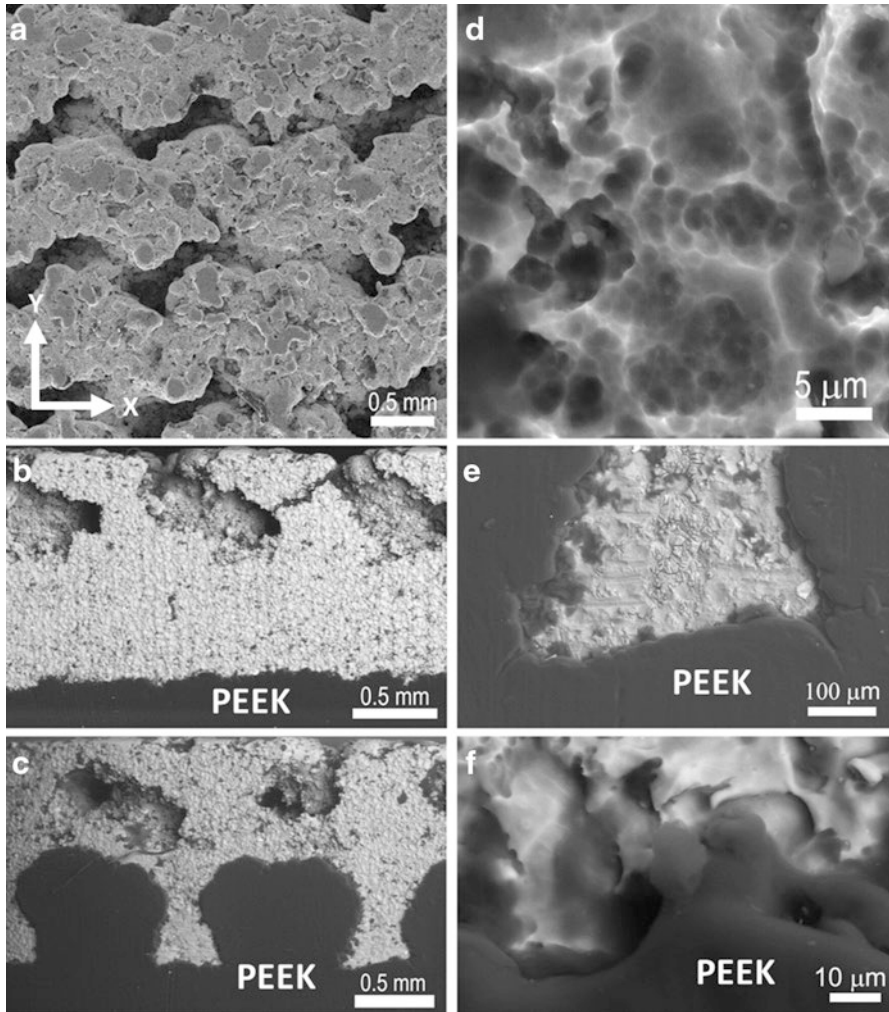
Fig. 5 SEM images of Ti6Al4V strut of the PTC device viewed from (**A**) the top and the side along direction (**B**) X and (**C**) Y; (**D**) a typical magnified SEM from the top view; (**E**) and (**F**) SEM images of the interface between Ti and PEEK along the Y and X direction, respectively

a well jointed interface between the Ti6Al4V endplate and the PEEK core of the PTC device (Fig. 5b, c, e, f).

High resolution SEM examinations showed the formation of nanostructures on the surface of the Ti6Al4V strut. Nano particles/features with a size of ~40 nm were observed in the rough regions of the surface (Fig. 6a), while nano pores with a size <10 nm were observed in the flat regions of the strut (Fig. 6b).
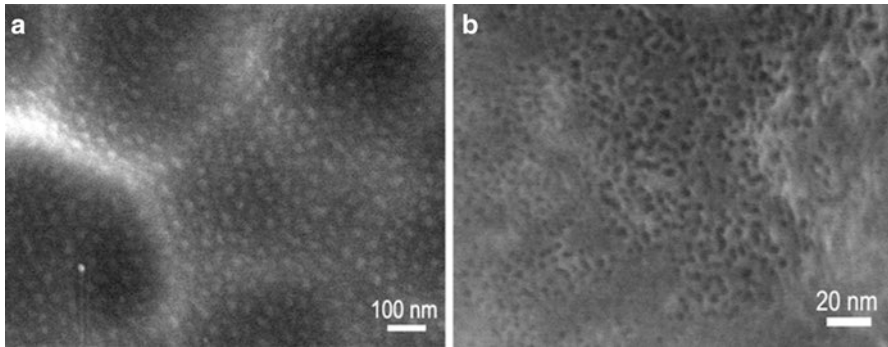
Fig. 6 Examples of high resolution SEM images of Ti6Al4V strut of the PTC device at various magnifications. (**a**) ×100,000 and (**b**) ×350,000

5   In Vitro Studies

In order to examine the effect of each of the structural components (PEEK, Ti6Al4V) on the proliferation and differentiation of the cells associated with building a solid fusion, the cellular responses of SAOS2 and MG63 cells (mature and immature osteoblasts, respectively) to the PTC components were examined. The cell lines were chosen to provide a larger phenotypical range to be examined, thereby enabling pre-osteoblast attachments to the endplates to be examined too. Specifically, the examinations were done on various individual substrates including the Ti6Al4V PTC endplate (Ti 3D), a planar Ti6Al4V surface (Ti 2D), and PEEK. The information presented on the immature osteoblast cell line (MG63) has previously been presented in part as an abstract at a scientific conference [48].

5.1   *Characterization of Ti 2D and 3D Substrates with SAOS2 Cells*

5.1.1   **Methods**

Substrates

Two different types of Ti6Al4V substrates were prepared. The first substrate (2D reference substrate, Ti 2D substrate) was made as a planar surface (disk with d = 12.7 mm, Mean Surface Roughness (Ra) ~ 12 ± 2 μm, See Fig. 7a). The second substrate (Ti 3D substrate) was similar to the PTC device endplates (similar topography, pore size, porosity, and material, See Fig. 7b). It was made as a 3D architecture with struts having an average diameter of 0.60 mm and macroporosity obtained with holes among the struts having diameter between 0.35 and 0.60 mm. Specifically,
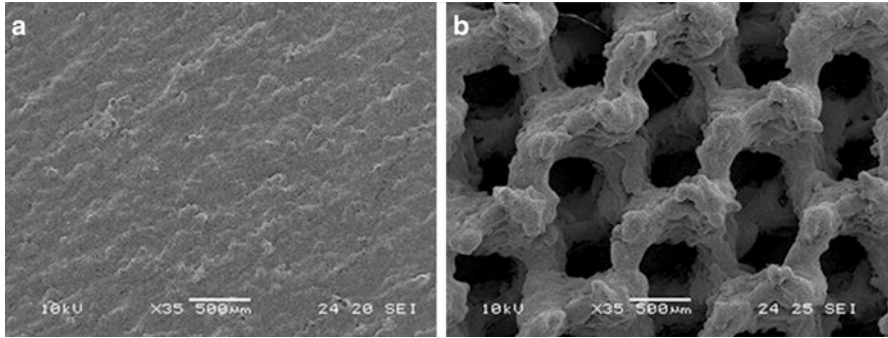
Fig. 7 SEM images of Ti6Al4V substrates. (**a**) Ti6Al4V 2D substrate and (**b**) Ti6Al4V 3D porous substrate (PTC endplate) used for in vitro characterization of SAOS2 cells

the structure had 50% porosity, 400-μm pore size, and 100% interconnectivity. The Ti 3D substrate (Fig. 7b) was manufactured so the surface on the struts appeared similar to the surface of the Ti 2D substrate.

Cells

The human osteosarcoma cell line SAOS2 (HTB85® ATCC™) was obtained from the American Type Culture Collection (Rockville, MD). For SAOS2 biocompatibility assays, the cells were cultured in McCoy's 5A modified medium with 1.5 mM l-glutamine and 25 mM HEPES (Cambrex Bio Science, Baltimore, MD), supplemented with 15% fetal bovine serum, 1 mM sodium pyruvate, 100 IU/mL penicillin, and 100 mg/mL streptomycin (proliferative medium). For SAOS2 complete differentiation to osteoblasts, 10^{-8} M dexamethasone, and 10 mM b-glycerophosphate (Sigma-Aldrich, Milwaukee, WI) were added. Ascorbic acid, another osteogenic supplement, is present as a component of McCoy's 5A modified medium (2.84 μM). The cells were cultured at 37 °C with 5% CO_2, routinely trypsinized after confluency, counted, and seeded onto the substrates.

Cell Seeding and Culture

The Ti substrates were sterilized with ethylene oxide at 38 °C for 8 h at 65% relative humidity. After 24 h of aeration to remove residual ethylene oxide, the substrates were placed inside a standard 24-well plate and were washed first with sterile distilled water, then with 0.9% NaCl sterile solution, and finally with culture medium. To ensure a maximum number of attached cells for substrates, a cell suspension of 6×10^5 cells was added in two steps onto the top of each substrate and, after 0.5 h, 1 mL of culture medium was added to cover the substrates. For biocompatibility
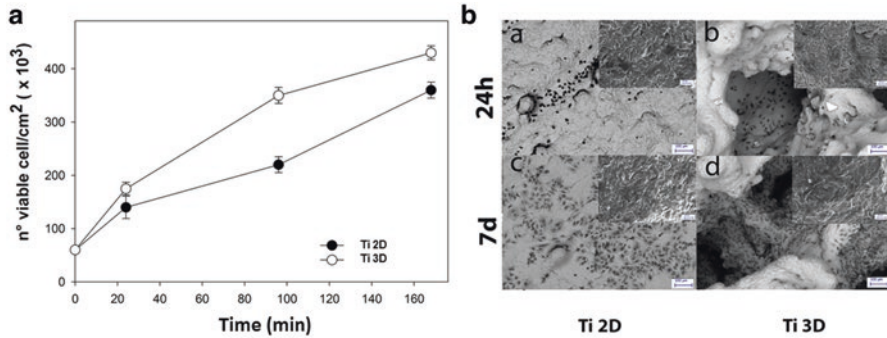
Fig. 8 Evaluation of SAOS2 cell viability and morphology on Ti 2D and 3D substrates. (**a**) MTT assay for cell viability using proliferative medium. (**b**) Cell morphology at 1 and 7 days of cell culture in proliferative medium. Scale bar in images is 100 μm

assays, the SAOS2 experiments were performed for 7 days in proliferative medium whereas the other parts of the SAOS2 experiment were conducted for 14 days in differentiative medium. The culture medium was changed every 3 days.

Evaluation of Cell Viability and Morphology on Ti Substrates

To evaluate the mitochondrial activity of the seeded cells, i.e., the cell viability on the Ti substrates, a test with 3-(4,5-dimethylthiazole-2-yl)-2,5-diphenyl tetrazolium bromide (MTT) (Sigma-Aldrich) was performed for the indicated times in proliferative medium (25, 95 and 170 min following seeding on substrates, Fig. 8a). Briefly, the culture medium was replaced by a 0.5 mg/mL solution of MTT in phosphate-buffered saline (PBS) and the cell cultures were incubated for 4 h. After removing the MTT solution, to solubilize the formazan bi-products, 500 μL of dimethyl sulphoxide (Sigma-Aldrich) were added, and the well plate containing the cultured Ti substrates was agitated for 20 min on a shaker. Aliquots of 200 μL were sampled, and the related absorbance values were measured at 570 nm by a microplate reader (BioRad Laboratories, Hercules, CA). In addition, cell morphology was investigated by SEM at days 1 and 7 (Fig. 8b).

Rabbit Polyclonal Antisera and Purified Proteins

A set of rabbit polyclonal antisera and purified proteins were obtained as previously reported [49].

Extraction of ECM Proteins from the Cultured Substrates and ELISA

On day 14, to evaluate the amount of the ECM constituents throughout the substrates surfaces, both the Ti substrates (2D and 3D) were washed with sterile PBS to remove the culture medium, and then incubated for 24 h at 37 °C with 1 mL of sterile sample buffer (20 mM Tris–HCl, 4 M GuHCl, 10 mM ethylenediaminetetraacetic acid, 0.066% [w/v] sodium dodecyl sulfate, pH 8.0). The sample buffer aliquots were removed, and then both types of Ti substrates (after 14 days of culture incubation) were centrifuged at 4000 rpm for 15 min to collect the sample buffer entrapped in the pores. The total protein concentration in both culture systems was evaluated by the BCA Protein Assay Kit (Pierce Biotechnology, Rockford, IL). After matrix extraction, the substrates were incubated, once again, for 24 h at 37 °C with 1 mL of sterile sample buffer, and no protein content was further detected. Calibration curves to measure type-I collagen, osteopontin, osteocalcin, and alkaline phosphatase (ALP) were performed. Microtiter wells were coated with increasing concentrations of each purified protein, from 10 to 2 μg, in a coating buffer (50 mM Na_2CO_3, pH 9.5) overnight at 4 °C. Control wells were coated with bovine serum albumin (BSA) as a negative control. To measure the ECM amount of each protein by an enzyme-linked immunosorbent assay (ELISA), microtiter wells were coated, overnight at 4 °C, with 100 μL of the previously extracted ECM (20 μg/mL in coating buffer). After three washes with PBS containing 0.1% (v/v) Tween 20, the wells were blocked by incubating with 200 μL of PBS containing 2% (w/v) BSA for 2 h at 22 °C. The wells were subsequently incubated for 1.5 h at 22 °C with 100 μL of the anti-type-I collagen, anti-osteopontin, anti-osteocalcin, and anti-ALP rabbit polyclonal antisera (1:500 dilution in 1% BSA). After washing, the wells were incubated for 1 h at 22 °C with 100 μL of horseradish peroxidase (HRP)-conjugated goat anti-rabbit IgG (1:1000 dilution in 1% BSA). The wells were finally incubated with 100 μL of the development solution (phosphate-citrate buffer with *o*-phenylenediamine dihydrochloride substrate). The color reaction was stopped with 100 μL of 0.5 M H_2SO_4, and the absorbance values were measured at 490 nm with a microplate reader (BioRad Laboratories). An underestimation of the absolute protein deposition is possible because the sample buffer, used for matrix extraction, contained sodium dodecyl sulfate, which may interfere with the protein adsorption during ELISA. The amount of ECM constituents throughout the Ti substrates was expressed as pg/(cells/substrates).

Indirect Immunofluorescence Staining

At the end of the culture period, the Ti substrates were fixed with 4% (w/v) paraformaldehyde solution in 0.1 M phosphate buffer (pH 7.4) for 8 h at room temperature and washed with PBS three times for 15 min. The substrates were then blocked by incubating with PBS-Albumin-Tween, PAT (PBS containing 1% [w/v] BSA and 0.02% [v/v] Tween 20) for 2 h at room temperature and washed. Anti-type-I collagen and anti-osteopontin rabbit polyclonal antisera were used as the primary

antibody with a dilution equal to 1:500 in PAT. The same dilution was performed with anti-FN rabbit polyclonal IgG. Incubation with the primary antibodies was made overnight at 48 °C, whereas the negative controls were incubated overnight at 4 °C with PAT. The substrates and the negative controls were washed and incubated with Alexa Fluor 488 goat anti-rabbit IgG (HþL) (Molecular Probes) at a dilution of 1:750 in PAT for 1 h at room temperature. At the end of the incubation, the substrates were washed in PBS, counterstained with a solution of propidium iodide (2 μg/mL) to target the cellular nuclei, and then washed. The images were taken by blue excitation (bandpass, 450–480 nm; dichromatic mirror, DM500; barrier filter, BA515) with a fluorescence microscope (BX51; Olympus, Tokyo, Japan) equipped with a digital image capture system (Olympus) at 20× magnification. The fluorescence background of the negative controls was negligible.

ALP Activity

ALP activity was determined using a colorimetric end point assay as previously described [50]. Briefly, an aliquot (1 mL) of 0.3 M p-nitrophenyl phosphate (PNPP, dissolved in glycine buffer, pH 10.5) was added to each substrate at 37 °C. After incubation, the reaction was stopped by the addition of 100 mL 5 M NaOH. Standards of PNPP in concentrations ranging from 0 to 50 mM were freshly prepared from dilutions of a 500 mM stock solution and incubated for 10 min with 7 U of ALP (Sigma-Aldrich) previously dissolved in 500 mL of ddH$_2$O. The absorbance reading was performed at 405 nm with a microplate reader (BioRad Laboratories) using 100 mL of standard or sample placed into individual wells of a 96-well plate. Samples were run in triplicate and compared against a calibration curve of p-nitrophenol standards. The enzyme activity was expressed as nanomoles of p-nitrophenol produced per minute per milligram of enzyme.

Statistical Analysis

A total of 30 Ti porous substrates were used for each repeated experiment (15 Ti 2D substrates and 15 Ti 3D substrates). Each experiment was repeated three times. Results are expressed as the mean ± standard deviation. Statistical differences were determined by unpaired two-tailed t tests with a significance level of $P < 0.05$.

5.1.2 Results

SAOS2 Cell Viability and Morphology

To evaluate the cell viability on Ti 2D and Ti 3D substrates during the culture period, a MTT test was performed (Fig. 8a). Interestingly, a higher cell attachment and proliferation was observed for the Ti 3D porous substrate relative to the Ti 2D
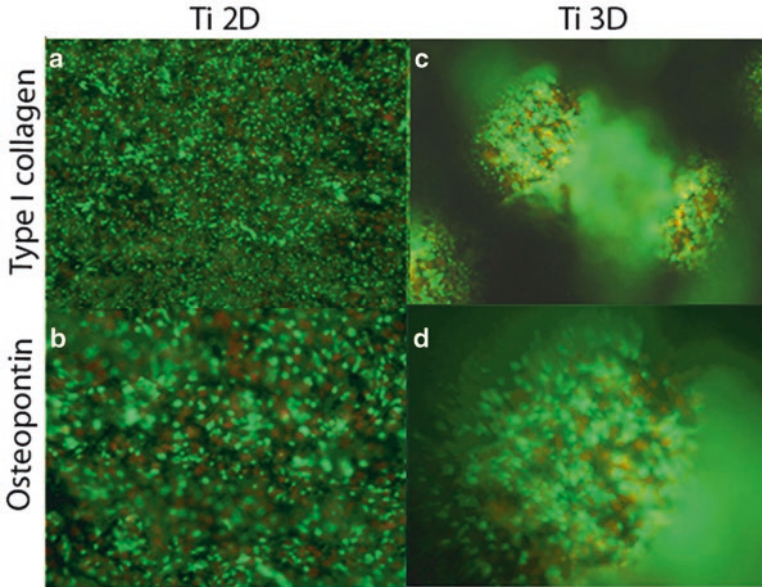
Fig. 9 Immunolocalization of type-I collagen (**a**, **c**) and osteopontin (**b**, **d**) on Ti 2D and Ti 3D substrates cultured with SAOS2 cells. Images captured at 20× magnification

substrate (Fig. 8a). SAOS2 cell morphology cultured on the Ti 2D and Ti 3D substrates was viewed by SEM (Fig. 8b). Representative images of 1 and 7 days of cell culture in proliferative medium shows adherence of cells to the surface of both types of substrates (Fig. 8b). In particular, the cells more homogeneously covered the surface and spanned to the neighboring fibers on the Ti 3D porous substrates than they did on Ti 2D substrate at 7 days (Fig. 8b). In general, more cells were observed on Ti 3D porous substrates relative to Ti 2D substrates at both incubation time points, confirming the MTT test. At higher magnification, no significant differences in cell morphology were observed on both types of substrates.

Characterization of the Bone Matrix Deposition

The total protein concentration was detected after 14 days of culture in differentiative medium. For the Ti 2D substrate, it was reported to be 412 ± 0.5 µg/mL and for the Ti 3D porous substrates, the protein content was 536 ± 1.1 µg/mL, respectively. To evaluate the effect of the substrate type to osseointegration and bone matrix deposition, SAOS2 cells were seeded on both types of substrates and cultivated for 14 days in a differentiative medium. At the end of cell culture, cell viability performed with MTT tests was higher on Ti 3D than on Ti 2D substrates (data not presented). Furthermore, the immunolocalization of type-I collagen (Fig. 9a, c),

Table 3 Normalized amount of the extracellular matrix constituents secreted and deposited throughout the substrates (* P < 0.05 for the comparison between the Ti 3D and Ti 2D substrates)

	Matrix proteins deposition after 14 days of SAOS2 cell culture in osteogenic medium expressed as pg/(cell/substrate)		
	Ti 2D	**Ti 3D**	**Ratio Ti 3D/ 2D**
Alkaline Phosphatase	4.08 ± 0.023	6.80 ± 0.014*	1.41
Osteocalcin	3.03 ± 0.021	4.90 ± 0.010*	1.62
Osteopontin	5.06 ± 0.021	7.06 ± 0.013*	1.40
Type I collagen	60.20 ± 0.022	76.00 ± 0.011*	1.30

and osteopontin (Fig. 9b, d) showed a slightly more intense green fluorescence on the Ti 3D porous substrates than on the Ti 2D substrates (Fig. 9).

The ECM extraction that was done to evaluate the amount of the ECM constituents produced throughout both types of Ti substrates showed a significantly higher deposition of bone proteins throughout the Ti 3D porous substrates in comparison with the culture on the Ti 2D substrates (P < 0.05) (Table 3). These data are in accordance with the immunofluorescence analysis performed on Ti 2D substrates and Ti 3D porous substrates (Fig. 9).

Specifically, a 41%, 62%, 40% and 30% enhancement of ALP, osteocalcin, osteopontin, and type-I collagen protein deposition was observed for the Ti 3D porous substrate relative to the Ti 2D substrate, respectively (Table 3). The enhancement of protein deposition was observed for ALP, which was 1.41 times greater for the Ti 3D porous substrate when compared with the Ti 2D substrate (Table 3). The ALP activity was measured on both types of substrates at the end of the culture period: the level of the ALP activity was significantly higher on the Ti 3D porous substrates (460 nmol/min/mg protein) than on Ti 2D substrate (280 nmol/min/mg protein) (P < 0.05).

5.2 Characterization of Ti 3D and PEEK Substrates with Human MG63 Cells

5.2.1 Methods

Substrates

Two different types of substrates were prepared. Similar to the 3D porous substrate for the SAOS2 in vitro experiment (Sect. 5.1), the primary substrate (Ti 3D substrate) was similar to the PTC endplates (similar topography, pore size, porosity, and material). The secondary substrate was a solid, smooth PEEK surface similar to

that used for the standard PEEK interbody spacers and for the core portion of the PTC devices (Sect. 2.2). The outer dimensions of each substrate were 19.05 mm (length), 19.05 mm (width), and 3.18 mm (height). The substrates were sterilized using an autoclave before their use in cell culture experiments. Control surfaces were standard tissue culture wells made from polystyrene (TCPS).

Cells and Assays

Human MG63 cells (ATCC; Manassas, VA) were thawed and cultured to confluence in standard tissue culture–treated flasks. At confluence, cells were passaged using trypsin and plated onto the PTC porous substrate, PEEK substrate, or TCPS surfaces. Density of plating was 3.24×10^4 cells per sample with the addition of 2 mL of cell culture media to each well (Dulbecco's modified Eagle's medium +10% fetal bovine serum +1% penicillin/streptomycin). Because of constraints in material availability, the PTC and PEEK substrates (with their respective individual TCPS controls) were plated at separate times. Seeding occurred for eight wells for each group. Media was changed 24 h after cell seeding and every 48 h thereafter for the duration of the study. Cells were cultured on the respective substrates for 7 days or until cells reached confluence on the TCPS control surface, after which conditioned media from each group was harvested in 15 mL centrifuge tubes and frozen at −80 °C for subsequent analysis.

   After collection and thawing of the conditioned media, secreted levels of BMP-2, BMP-4, BMP-7, TGF-β1, and VEGF-A were determined by an ELISA using commercially available kits per the manufacturer's instructions (DuoSet ELISA Development Systems, R&D Systems, Minneapolis, MN). Secreted levels of osteocalcin were also determined by ELISA (Osteocalcin Human Direct ELISA Kit, Life Technologies, Carlsbad, CA) following the manufacturer's instructions. Total protein levels in the cell lysate were determined for normalization of secreted protein levels (Pierce BCA Protein Assay). Ratios for the levels of each secreted protein (pg growth factor/μg total protein) on the respective substrates were calculated. Substrate/control ratios were calculated from the ratio between each individual substrate sample secretion level and the total average of the associated control (TCPS) secretion level.

Statistical Analysis

Means and standard deviations (SDs) for normalized protein secretion levels were calculated. Statistical differences between substrate and control secretion levels, and between PTC and PEEK substrate/control ratios, were determined by unpaired two-tailed t tests with a significance level of $P < 0.05$. All results are presented as mean ± SD.
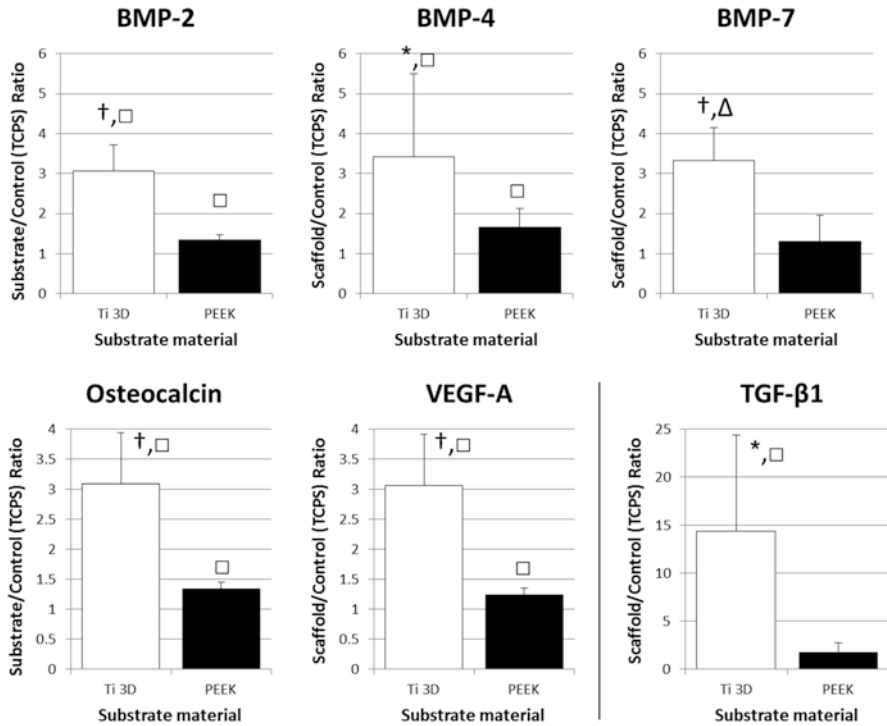
Fig. 10 Substrate/control (TCPS) ratios for the expression of growth factors on either Ti 3D substrates or PEEK substrates at Day 7. Top row: BMP-2, BMP-4, and BMP-7 (growth factors involved in osteogenesis); bottom row: osteocalcin, TGF-β1, and VEGF-A (growth factors involved in osteoblast differentiation and maturation). Statistical significance is indicated for Substrate/Control Ratio comparisons (*P < 0.05, †P < 0.001) and substrate vs. associated control (TCPS) comparisons (□ P < 0.01, Δ P < 0.001)

5.2.2 Results

Comparisons of Secretions from Ti/PEEK Substrate Versus Control Surfaces

Secretions from cells grown on Ti and PEEK substrates, compared with TCPS control values, are presented in Fig. 10. Levels of the osteogenic growth factors BMP-2 and BMP-4 were significantly increased from cells plated onto both Ti 3D and PEEK substrates (all $P \leq 0.01$). Levels of BMP-7 secretion were significantly higher in cells plated on the Ti 3D substrate ($P < 0.001$), but not the PEEK substrate ($P = 0.49$), compared with TCPS controls. The secretion of markers of osteoblast differentiation and maturation was also examined (Fig. 10). Levels of osteocalcin and VEGF-A were significantly increased in cells plated onto both Ti 3D and PEEK substrates compared to TCPS controls (all $P < 0.01$). Levels of TGF-β1 secretion from cells plated on the Ti 3D substrate, but not the PEEK surface, were also significantly increased compared with controls ($P < 0.01$ vs. $P = 0.14$, respectively).

Comparisons of Secretions from Ti 3D Versus PEEK Surfaces

The substrate/control ratios for each of the osteogenic growth factors measured are presented in Fig. 10. Increases in ratios for BMP-2, BMP-4, and BMP-7 (2.3-, 2.1- and 2.6-fold, respectively) were significantly greater ($P < 0.001$, $P = 0.04$, $P < 0.001$, respectively) for the Ti 3D substrate than the PEEK substrate, suggesting an enhanced osteogenic response for the Ti 3D porous substrate. Figure 10 presents substrate/control ratio data for each of the growth factors associated with osteoblast differentiation and maturation. The increase in the respective substrate/control ratios was significantly greater for the Ti 3D substrate than the PEEK substrate for osteocalcin (2.3-fold, $P < 0.001$), TGF-β1 (8.2-fold, $P = 0.007$), and VEGF-A (2.5-fold, $P < 0.001$).

6 In Vivo Animal Studies

Based on the in vitro evidence that the PTC endplate leads to an increased osteogenic environment (Sect. 5) an in vivo examination of the components of the PEEK and PTC devices was performed in a rabbit model. This was done to determine bone ingrowth capability into the pores of the PTC endplate and to examine biocompatibility of the PTC components. Lastly, an in vivo large animal (ovine) study was performed to examine the fusion capability of a full clinical PTC device. This large animal study would furthermore give insight into how the PTC device differentiated itself from a standard PEEK interbody device with respect to fusion quality and fusion mass generation. The information presented on the two animal models have previously been presented in part as abstracts at scientific conferences [51, 52].

6.1 Characterization of Ti 3D and PEEK Substrates in a Rabbit Animal Model

6.1.1 Methods

Substrates for Implantation

The implants used for this in vivo experiment were 3.3-mm cylindrical rods (3.1-mm diameter) made of either Ti6Al4V (porous substrate, with 50% porosity, 400-µm pore size, and 100% interconnectivity) or PEEK (solid, smooth surface) which were similar in properties to the endplates and PEEK core of the PTC interbody devices (Sect. 2.2), respectively. Similar to the 3D porous substrate used for both in vitro experiments (Sect. 5), the Ti6Al4V implant is referenced as the Ti 3D substrate.

Animals

A total of 13 New Zealand white rabbits ≥9 months of age were evaluated in this study. The local Institutional Animal Care and Use Committee (IACUC) of T3Labs (380 Northyards Blvd NW, Atlanta, GA 30313) reviewed and approved this study (study code: OF01B). Per the approved protocol, animals were handled and maintained in accordance with the requirement of the Animal Welfare Act and its amendments [53]; procedures conformed to standards of the Guide for the Care and Use of Laboratory Animals [54]. Animals were observed at least once daily.

Surgery

Animals were assigned to 1 of 6 cohorts: 1) baseline, Ti 3D substrate (n = 2); 2) 4-week, Ti 3D substrate (n = 2); 3) 8-week, Ti 3D substrate (n = 2); 4) baseline, PEEK substrate (n = 3); 5) 4-week, PEEK substrate (n = 2); and 6) 8-week, PEEK substrate (n = 2). Each animal was scheduled to receive 4 implants of similar material, resulting in 2 implants per leg. Due to surgical complications, 2 of the baseline animals (PEEK group) only received implants unilaterally. Thus, the total number of inserted substrates was 8 for each time point and implant material combination (i.e., a total of 24 Ti 3D and 24 PEEK substrates). On the day of implantation, sedated animals were incised on the medial side of the tibia and fasciae were dissected. The right and left tibia of each rabbit was used. Drill bits (diameter, 2.5–3.1 mm) were used to predrill holes with saline irrigation. A proximal hole was placed 3 mm distal to the epiphysial growth plate; a distal hole was placed approximately 10 mm distal to the proximal hole, but within the metaphyseal region. Holes were sized to ensure that substrates were flush with the periosteal surface. Substrates were inserted using the press-fit technique, oriented perpendicularly to the long axis of the bone. Incisions were sutured in 2 layers and bandaged; correct substrate positioning was confirmed radiographically.

Assessment

Animals were euthanized at protocol-directed time points. Bilateral tibias were harvested and immersed in 10% neutral buffered formalin and sent for histological, morphometric, and microscopic analysis (Alizée Pathology LLC, Thurmont, MD, USA). Implant sites were embedded in methylmethacrylate and sectioned longitudinally, achieving the largest possible cross section of the implants in order to avoid a false high ingrowth percentage. A single section from each specimen, which included the center axial cut of two implants, was chosen for bone ingrowth evaluation. Unstained slides were etched and stained with hematoxylin and eosin. Tibial Ti 3D porous substrates (proximal and distal) were evaluated for bone ingrowth into the top cortical interface of the implant area. This region of interest was defined as

the area within 1000 µm from the "top" surface of the substrate. Only substrates for which this region of interest was within the cortical region were included. In addition, bone apposition for the cortical region was determined for both PEEK and Ti 3D substrates. Quantification of bone apposition was done by evaluating the percent outer surface length in direct contact with bone. Histomorphometry was performed using Image-Pro® Plus software (Media Cybernetics, Rockville, MD, USA). Pathological evaluation of wound healing on each slide for both Ti 3D and PEEK substrates was conducted by a veterinarian. Per ISO 10993 (Biological evaluation of medical devices) scoring for inflammation, polymorphonuclear cells, lymphocytes, plasma cells, macrophages, and foreign body giant cells were assessed using a scale from 0 to 4 (0 = none; 1 = 1–5 per 400× field; 2 = 6–15 per 400× field; 3 = 16–25 per 400× field; 4 = ≥26 per 400× field). Necrosis was assessed as absent (0), minimal (1), mild (2), moderate (3), or severe (4). Fibrous capsule formation was assessed as absent (0), narrow (1), moderately thick (2), thick (3), or extensive (4). The total irritancy score was calculated as ([inflammation + necrosis] × 2 + fibrous capsule formation) for one slide for each implant. Irritant status was assessed as nonirritant (0.0–2.9), slight irritant (3.0–8.9), moderate irritant (9.0–15.0), and severe irritant (>15.0). Specimens where nondevice-related inflammation and tissue irritation presented were not included in the pathological evaluation. In total, the following group sizes were evaluated: baseline/Ti 3D, n = 8; 4-weeks/Ti 3D, n = 8; 8-weeks/Ti 3D, n = 8; baseline/PEEK, n = 8; 4-weeks/PEEK, n = 6; and 8-weeks/ PEEK, n = 8.

Statistical Analysis

The means and standard deviations for bone ingrowth, bone apposition and irritancy scores were calculated. Statistical differences were determined by unpaired two-tailed t tests with a significance level of $P < 0.05$. Differences between baseline and week 8 values for bone ingrowth and apposition for Ti 3D substrates and differences in irritancy scores between Ti 3D and PEEK substrates were assessed.

6.1.2   Results

Bone Apposition and Ingrowth in the Cortical Region

No ingrowth data were calculated for the week-4 group because the majority of the Ti 3D substrates were below the cortical surface. This resulted in the following implant group sizes: baseline, n = 8; 8-weeks, n = 8. At week 8, the Ti 3D substrate showed significant ingrowth of bone within the top cortical interface relative to baseline (36.5% vs 0%, respectively, $P < 0.001$). Bone apposition in the cortical region at 4 and 8 weeks was found to be similar between the PEEK and Ti 3D substrates (19.6% vs. 16.3% and 29.4% vs. 35.6%, respectively).
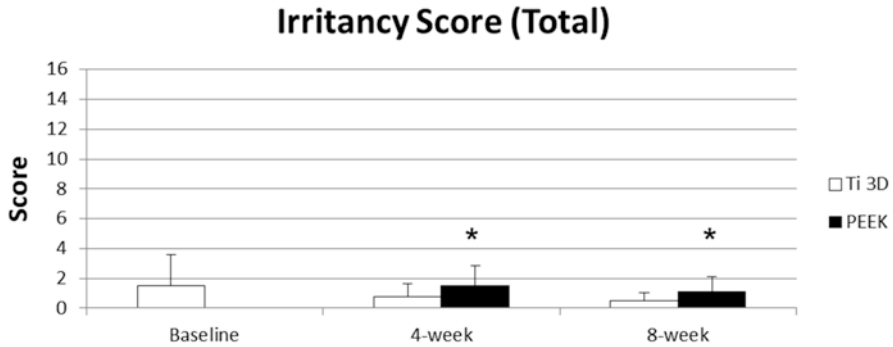
Irritancy Score (Total)

Fig. 11 Pathological irritancy score evaluation of rabbit tibial implants made from poly-ether-ether-ketone (PEEK) and 3D porous Ti6Al4V. Scores were derived for the entire implant evaluation. Classification of scoring (per ISO 10993): nonirritant (0.0–2.9), slight irritant (3.0–8.9), moderate irritant (9.0–15.0), and severe irritant (>15.0). Statistical significance is indicated for Baseline vs. time point (*P < 0.05)

Biocompatibility and Irritancy

Both Ti 3D and PEEK substrates had nonexistent or minimal inflammatory response along their surfaces (Fig. 11). The Ti 3D porous substrate showed no inflammation at 4 or 8 weeks (Fig. 11). Because of the low severity of inflammatory infiltrate around some of the PEEK substrates and the concurrent and confounding observation of normal hematopoiesis in the adjacent bone marrow, infiltrates could not be ascribed to a reactive inflammatory process to the implant; under these conditions, both substrates were considered to be nonirritant. There were no differences observed between Ti 3D and PEEK substrates in irritancy scores at any time point. There was no change in irritancy scores across time for the Ti 3D substrate. There was a slight but significant increase in total irritancy score from baseline to weeks 4 and 8 (both $P = 0.01$) for PEEK substrates, although PEEK was still considered a nonirritant (Fig. 11). Both substrates showed a slight fibrous capsule formation along their surfaces. There was no evidence of sequestration in any group.

6.2 Evaluation of a PTC Interbody Device in an Ovine Lumbar Fusion Model

6.2.1 Methods

Animals, Devices and Surgery

All animal procedures were performed at an accredited hospital for veterinary medicine (Colorado State University, Fort Collins, CO) under a protocol approved by the local Institutional Animal Care and Use Committee (study code: SRL 15-08).

Per the approved protocol animals were handled and maintained in accordance with the requirement of the Animal Welfare Act and its amendments [53]; procedures conformed to standards of the Guide for the Care and Use of Laboratory Animals [54].

Thirty-four (34) mature female sheep (weighing 65–103 kg and all 3+ years of age) underwent instrumented interbody fusion at L2-L3 and L4-L5, with each animal having one level treated with FORZA PTC (Fig. 2a) and the other with FORZA PEEK (Fig. 2b) using a left lateral retroperitoneal approach (Fig. 12). The location (L2-L3 or L4-L5) was randomized between each animal. For supplemental fixation, the Orthofix FIREBIRD® pedicle screw system was used (4.5 × 30 mm polyaxial screws, 5 mm rod). The graft window of the interbody cages was filled with an iliac crest autograft harvested during device implantation.

The implants had similar size with a footprint of 9 mm x 23 mm x 7 mm (width x length x height), 0 degrees of lordosis, and a 0.3 cc central opening. Eight (8) animals were sacrificed at each time point, which included baseline, 8, 12 and 16 weeks post-surgery. Baseline (0 weeks) animals were done using fresh cadavers from another study.

Assessments

Post sacrifice, animal spines were carefully dissected and separated into each functional spine unit (FSU, i.e., L2-3 and L4-5, Fig. 12b). Each FSU underwent non-destructive biomechanics testing yielding range of motion (ROM) and stiffness. This was done using pure moments up to 6 N-m in flexion-extension, lateral bending and axial rotation without applying off-set moments or forces. The resulting moments were captured using a six degree-of-freedom transducer (AMTI, Watertown, MA). Following biomechanical testing each FSU was fixed in 10% neutral buffered formalin (NBF) for a week and then underwent microcomputed tomography (microCT) scanning at a resolution of 37 μm yielding bone volume fraction (BV/TV) and bone mineral density (BMD) within the graft window of each device (Fig. 13, region 1). MicroCT was not performed for the baseline animals.

Following microCT scanning, each FSU underwent histologic processing and hard-tissue sectioning with two distinct sections per FSU cut in the sagittal plane. Histomorphometry was performed for each section for each FSU yielding core (Fig. 13, region 1), superior/inferior surface region (Fig. 13, region 2) bone and soft tissue area fraction. The bone ingrowth into PTC endplate pores was also calculated.

Finally, a qualitative scoring of the fusion based on the microCT and histology sections was done using four (4) independent and blinded reviewers. The fusion score was determined using a 5-point scale with a score of 1 indicating a non-union and a score of 5 indicating total bridging of the graft window with calcified tissue (Table 4).
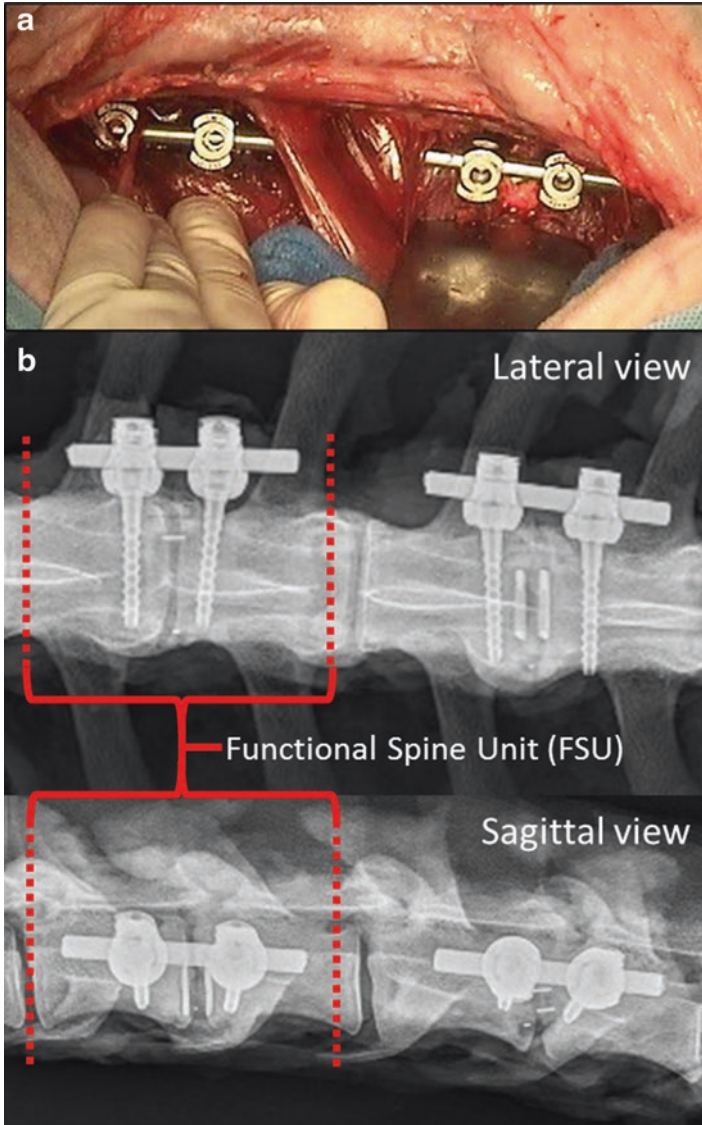
Fig. 12 Implantation of FORZA PTC and FORZA PEEK at L2-L3 and L4-L5. (**a**) Surgical technique using a lateral retroperitoneal approach. Supplemental fixation was done as shown using the Orthofix FIREBIRD® pedicle screw system. (**b**) Lateral and sagittal post-surgery radiographs indicating each Functional Spine Unit (FSU)
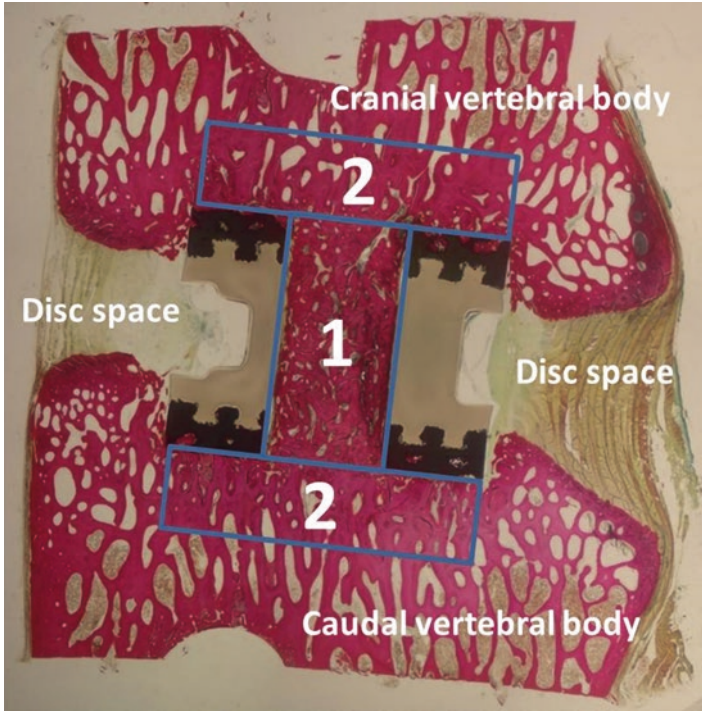
Fig. 13 Histologic sagittal cut section of the PTC device with the disc space, cranial and caudal vertebral bodies indicated. Histologic region of interests (ROI) indicated for (1) core section and (2) cranial and caudal implant surfaces. ROI 2 extended 0.25 mm above and below the PTC endplates

Table 4 Qualitative fusion score used for microCT and histology images of the core fusion mass within the PTC device

Fusion score	Fusion quality/connectivity
1	Non-union
2	Partial bridging with large gaps (up to 1.00 mm) in the calcified tissue structure
3	Partial bridging with medium gaps (up to 0.50 mm) in the calcified tissue structure
4	Partial bridging with small gaps (up to 0.25 mm) in the calcified tissue structure
5	Total bridging of the graft with calcified tissue

Statistical Analysis

For graphing purposes, PTC values were normalized to the PEEK values for the corresponding outcome measure and time point (PEEK = 100%). Graphs illustrate mean ± standard error. A 2-way analysis of variance (ANOVA) was used for each variable (time and device) with a Bonferroni post-hoc test. Significance was set at $P < 0.05$.
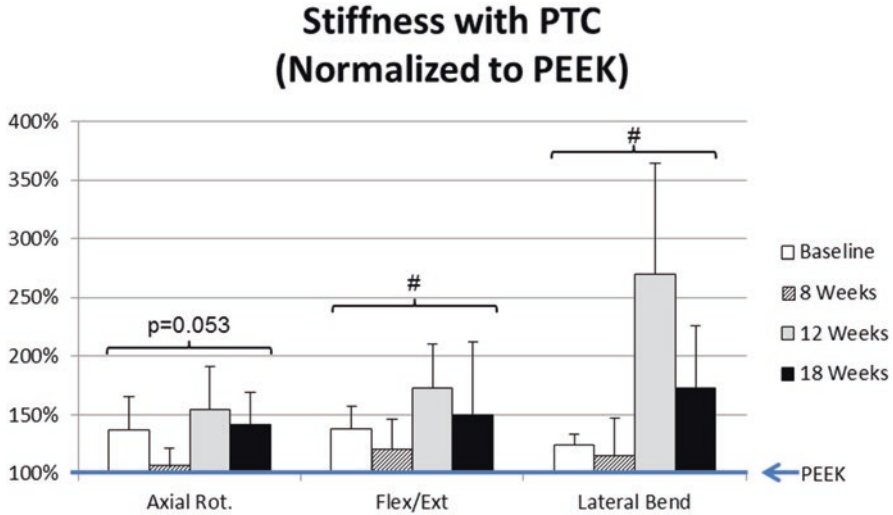
Fig. 14 Qualitative normalized stiffness for PTC device for all three biomechanical tests. Each represented PTC stiffness was normalized to the PEEK average stiffness for the corresponding loading pattern and time point. Pound-sign (#) indicates that the PTC group had significantly greater stiffness than the PEEK group across time ($P < 0.05$, 2-way ANOVA)

6.2.2 Results

Animal Health

Animals were monitored daily with no abnormal findings attributed to the investigational implants.

Biomechanical Properties

Biomechanics showed that across time the PTC group had a significantly greater stiffness than the PEEK group for flexion/extension and lateral bending (Fig. 14) which was accompanied by a decrease in range of motion (lateral bending: $P \leq 0.01$; flexion-extension: $P = 0.02$) between 8 and 18 weeks. Although axial rotation only showed a great trend in the difference between PTC and PEEK across time (Fig. 14), PTC was the only one to show a significant increase between 0 and 18 weeks, and 8 and 18 weeks ($P \leq 0.01$). Similarly to the other loading directions this was accompanied by a significant decrease in range of motion for PTC ($P = 0.01$).
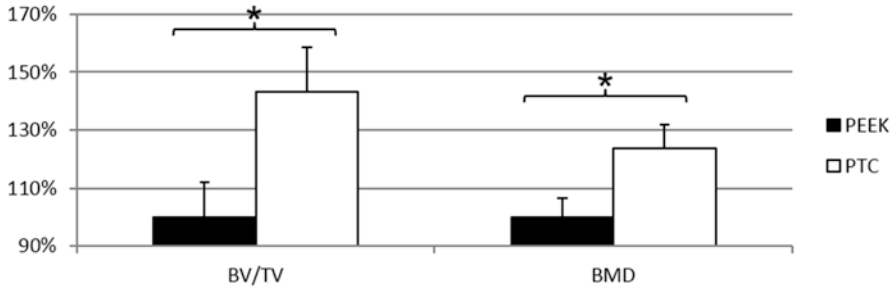
Fig. 15 Normalized microCT outcome measures for graft window of implant devices: Normalized bone volume density (BV/TV) and bone mineral density (BMD) at 8 weeks post-surgery. Each represented microCT outcome measure was normalized to the PEEK average for the corresponding microCT outcome measure and time point. *Asterisks* (*) indicate significant difference between PEEK and PTC (P < 0.05, Bonferroni post-hoc)

MicroCT

MicroCT analysis showed a significant increase in bone volume density and bone mineral density (43% and 24%, respectively) in the graft window at 8 weeks for PTC vs. PEEK (P = 0.04 and P = 0.02, respectively; Fig. 15).

Histology

Histological analyses showed that the percent bone present in the graft window was significantly greater for PTC than PEEK at 8 weeks (51% vs. 36%, P = 0.05; Fig. 16). In addition, there was a significant decrease in soft tissue for PTC compared to PEEK at 12 weeks (29% vs. 42%, P < 0.05).

Furthermore, it was shown that the superior (cranial) and inferior (caudal) endplates of the PTC implant had greater bone presence with less soft tissue than the PEEK endplates (P < 0.05, Fig. 17).

Additionally bone ingrowth into the porous PTC endplates was found to be 47.4 ± 3.2%, 46.3 ± 4.7%, and 41.4 ± 2.6% at 8, 12 and 16 weeks post-surgery, respectively
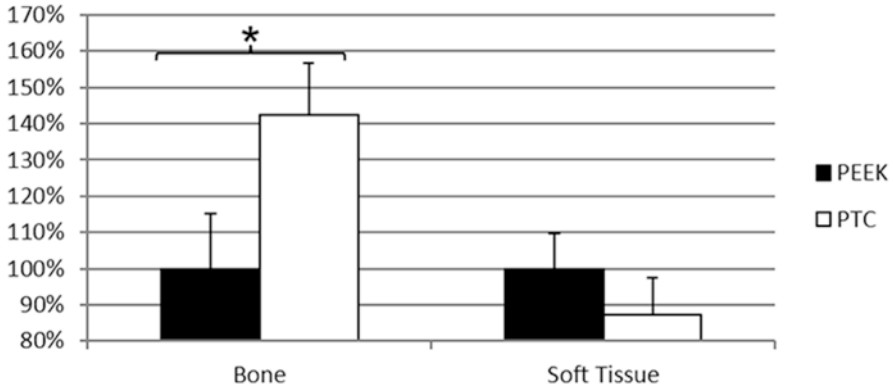
Fig. 16 Histology outcome measures for graft window of implant devices: Normalized bone and soft tissue fraction at 8 weeks post-surgery. Each represented histology outcome measure was normalized to the PEEK average for the corresponding histology outcome measure and time point. *Asterisks* (*) indicate significant difference between PEEK and PTC (P < 0.05, Bonferroni post-hoc)
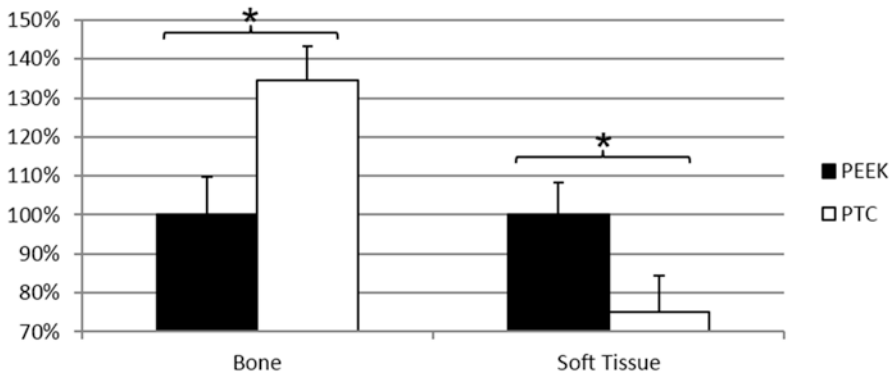

Fig. 17 Histology outcome measures for superior (cranial) and inferior (caudal) surfaces for the implant devices: Normalized bone and soft tissue fraction at 8 weeks post-surgery. Each represented histology outcome measure was normalized to the PEEK average for the corresponding histology outcome measure and time point. *Asterisks* (*) indicate significant difference between PEEK and PTC (P < 0.05, Bonferroni post-hoc).
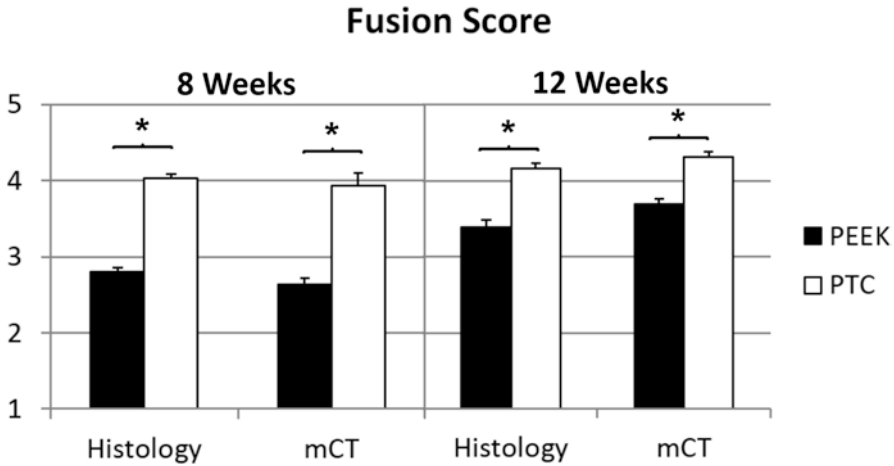
Fig. 18 Fusion score for implant device based on microCT and histology images at 8 and 12 weeks post-surgery. *Asterisk* (*) indicate significant difference between PEEK and PTC for the particular image modality (P < 0.02)

Fusion Score

Fusion scores were found to be significantly greater for PTC relative to PEEK at both 8 and 12 weeks using both the microCT and the histology images (Fig. 18). PEEK fusion scores, however, were the only ones to increase over time, which was expected since PTC achieved higher fusion scores at the early time points.

7　Discussions

This novel PEEK Titanium Composite (PTC) interbody device was developed in order to combine the advantages from both PEEK and titanium/tantalum spine fusion interbody devices by employing a PEEK center with titanium alloy (Ti6Al4V) endplates made from a novel 3D titanium mesh pattern. In order to examine the mechanical characteristics relative to a standard PEEK device and to further characterize the components of this novel device and the device as a whole several investigations were performed including mechanical, in vitro and in vivo assessments.

　While the mechanical tests were done to examine the mechanical properties of the full PTC device relative to a PEEK device, the surface topography examinations were done to illustrate the added surface roughness feature of the PTC endplates. As discussed previously, surface roughness has been correlated with an increased osteogenic environment [45, 46], so the in vitro tests were chosen to examine the static biological effects of the porous titanium surface versus a standard PEEK surface. The first in vivo study (Sect. 6.1) was chosen to further examine the two types

of surfaces in a native biological environment while being subject to loading due to normal animal activity. Lastly, the large animal in vivo study (Sect. 6.2) was performed to examine the fusion capability of a full clinical PTC device and give insight into how a PTC device differentiate itself from a standard PEEK interbody device with respect to fusion quality and fusion mass generation.

The mechanical testing results (Sect. 3) indicate that the PTC device has higher yield loads for all testing modes when compared to a standard marketed PEEK device. This indicates that the composite structure has a robust bonding between the porous titanium endplates and its PEEK core (Fig. 3c), which was supported by the inter-digestion layer examination in Sect. 4 (Fig. 5). From a mechanical perspective, the PTC device is therefore expected to perform similarly to PEEK in an in vivo setting as was shown in Sect. 6.2. One potential limitation to the mechanical testing was that the shallow pocket may have constrained the expansion experienced by the device during compression. However, this configuration gave an even higher stress at the interface between the porous titanium layer and the PEEK core for the PTC device which created a worst case testing scenario for the interface which still revealed higher yield loads than the standard PEEK device.

The surface typography AFM examination of an individual Ti6Al4V strut from the PTC endplate showed a micro-roughness range from 1.77 to 7.83 μm depending on the surface toughness parameter, which would give expectations of an increased osteogenic environment at the endplate [45, 46]. The surface roughness was furthermore correlated with SEM images of the strut surfaces, which showed two types of nano-structures were present in the sample depending on the roughness. Finally, the SEM images of the PTC also showed a solid joint of the PEEK core and the Ti6Al4V endplate plate at the inter-digitation layer, which correlated well with the mechanical results in Sect. 3.

Based on the surface roughness of the individual Ti6Al4V struts found in Sect. 4, the in vitro studies set out to show that this would lead to an increased osteogenic environment. Specifically, the first in vitro test of the Ti 3D PTC endplates involved the human SAOS2 cell line which was selected as it exhibits several fundamental osteoblast characteristics [55] and represents a widely used model for the in vitro study of osteoblasts. Previously, it has been reported that an increase in bone formation depends on the enhancement of ECM synthesis [56]. The examined components of the ECM included ALP, type-I collagen, osteopontin, and osteocalcin, which are implicated in bone formation and remodeling. ALP makes phosphate available for calcification, while bone type-I collagen, designated [alfa1(I)2alfa2], comprises 85–90% of the total organic bone matrix, and its synthesis is upregulated at the proliferation stage and downregulated during the subsequent stages [57, 58]. Osteopontin, a glycosylated phosphoprotein, plays an important role in cell attachment [59] and calcification of mineralized tissue [60]; osteocalcin, a member of the bone Gla protein family [61], is the latest of the secreted ECM protein and constitutes 1–2% of the total bone protein. As it was shown, cell seeding and cultivation on Ti 3D porous substrates showed a significant increase in the ECM components produced by mature SAOS2 osteoblasts relative to the Ti 2D substrates (Table 3, Fig. 9). Specifically, the 30% increase in type-I collagen is similar to what others

have shown using commercially pure titanium plasma sprayed substrates (~30% relative to 2D Ti substrate at 96 h in culture) [62]. In view of the increases in ECM components, and paired with the observation that the 3D porous surface had higher cell attachment and proliferation (Fig. 8a), the 3D porous substrate would be expected to be a better substrate (relative to a planar 2D substrate) for increasing osteoblast maturation and bone formation in vivo. For the in vitro tests involving the SAOS2 cell line, the increase in calcium deposition was consistent with the increase in ALP expression for the Ti 3D porous substrates relative to the Ti 2D substrates (Table 3). The positive correlation between ALP and relative surface roughness (Ti 2D vs. Ti 3D) is also consistent with what has previously been shown for smooth vs. sand blasted (Ti 2D) vs. plasma sprayed (Ti 2.5D) titanium surface [62], or machined vs. rough Ti6Al4V surfaces [63]. We hypothesize that the expression of the membrane-bound ALP protein on the osteoblasts initiates the mineralization of the matrix, which is supported by previous in vivo studies which have shown significant expressions of ALP in osteoblasts [64], an in in vitro differentiation studies with osteoblast-like cell lines [65]. The high expression of ALP and of osteopontin may therefore suggest that the osteoblasts on the Ti 3D porous substrate are more differentiated than on the Ti 2D substrate and have already initiated bone ECM deposition.

Electing to examine the response of a second cell line (human MG63 cells) to the Ti 3D PTC endplate was due to the SAOS2 cell line being a more mature osteoblastic phenotype [66]. The MG63 cell line is an immature osteoblast [66] which would provide a larger phenotypical range to be examined, thereby enabling pre-osteoblast attachment to the Ti 3D substrate to be examined too. As the results indicate osteoconduction, as measured by the secretion of growth factors involved in the creation and maturation of bony tissue [25, 26] which was significantly improved with the Ti 3D porous substrate compared with PEEK alone and importantly for each substrate relative to controls (Fig. 10). The percent increase in secreted growth factors from human MG63 cells (relative to TCPS control) for the Ti 3D substrate was furthermore found to be slightly higher than that presented in previous studies examining rough 2D Ti6Al4V surfaces (310% vs. ~260% for BMP-2, 340% vs. ~180% for BMP-4, 330% vs. ~240% for BMP-7, and 310% vs. ~210% for osteocalcin) [29]. Relative to other 3D Ti6Al4V substrate of similar porosity and pore size, the percent increase in secreted growth factors were similar for BMP-2, BMP-4, osteocalcin and VEGF-A [67]. Altogether, this may indicate that although the standard PEEK or a rough 2D titanium surface may provide an increase in osteoconduction, the Ti 3D endplate could potentially provide a surface substrate with an even better osteoconductive potential.

Paralleling the two in vitro tests, the in vivo examination of the PEEK and Ti 3D components of the PTC device (Sect. 6.1) showed the Ti 3D porous substrate having a significant bone ingrowth capability at week 8, in addition to similar bone apposition relative to the PEEK implant. The amount of ingrowth at week 8 (36.5%) was found to be similar to what other studies have shown using similar porosity and pore sizes for porous Ti6Al4V substrates albeit in different implant locations (qualitatively the same at 8 weeks in the rabbit cranium) [68] and species (18–25% at

12 weeks in the goat vertebrae) [69]. The significant bone ingrowth was most likely due to its porous, irregular surface, offering many points of bone contact. As shown in the in vitro tests (Sect. 5) and the literature, such porous surfaces have been associated with signaling environments that are favorable for enhancing the osteoblast maturation required for fusion of the implant with surrounding bone [29]. The rough surface of the Ti 3D porous substrate (Sect. 4), like other roughened titanium alloy surfaces and unlike the solid PEEK surface, would therefore be expected to favorably influence osteoconduction and osteomaturation [22, 29]. Furthermore, it was noted that the bone apposition was lower at 8 weeks compared to 4 weeks for both implants. This was expected due to extensive remodeling between week 4 and week 8. In addition, the in vivo examinations showed the Ti 3D porous substrate having similar biocompatibility as PEEK, which was expected (Fig. 11). Note that the in vivo study presented in Sect. 6.1 has certain limitations, which include the specimen transplant locations for the in vivo evaluation of the device components (Sect. 6.1). Several of the Ti 3D cylindrical porous substrates were placed in a region void of trabecular bone leading to no bone ingrowth in the medullary region of the implant as it would be expected since bone ingrowth only occurs if several criteria are fulfilled including the need for the implant be in close contact with the host bone [70]. Thus, the evaluation of only the implant region in contact with cortical bone provided a more fair assessment of the ingrowth capabilities of the implant, which is in accordance with what has been done in other studies examining bone ingrowth in implants spanning the cortex and medullary space [71–73].

Lastly, the large animal in vivo study (Sect. 6.2) showed that relative to a standard PEEK interbody device, the PTC device led to a significant reduction in range of motion and significant increase in stiffness. These biomechanical findings were reinforced by the presence of significantly more bone in the graft window, ingrowth into the novel endplates and significantly higher fusion scores. In addition, the radiolucent PEEK mid-portion of the PTC implant allowed for plain radiographic determination of bone graft maturation and solidification through its central core (Fig. 12b) as expected.

In all, the novel endplates of the PTC device composite structure provides an enhanced expression of growth factors from immature and mature osteoblast in vitro, indicating a favorable environment for osteoblast recruitment, maturation and bone repair. This improvement in osteogenic environment for the Ti 3D endplates may be due to the proven surface roughness and strut nano-structures. The increased osteogenic environment has also been seen for roughened 2D titanium surfaces [29]. However, the nature of the 2-D surface does not allow for efficient anchoring of the adjacent bone relative to surfaces such as a 3D mesh through which bone can grow, evidenced by the significant osteointegration response provided by the Ti 3D endplate. Thus, by combining an osteoconductive surface with a 3D geometry, the resulting amount of bony ingrowth on the Ti 3D endplate gives the novel PTC interbody device the potential for better bone ongrowth and ingrowth relative to a standard PEEK device as indicated in the ovine in vivo study (Sect. 6.2).

8 Conclusions

The PTC technology has been successfully applied to several standard PEEK interbody devices and subsequently been approved by the FDA. The endplate components of the novel PTC interbody device provide solid substrates that are biocompatible and topographically designed to provide a favorable biochemical environment for the formation of new bone tissue ingrowth within a surgical site relative to a standard PEEK device. In addition, the PTC interbody device provides a PEEK/Titanium composite as structurally sound as a standard PEEK device and with a radiolucent PEEK mid-portion allowing for plain radiographic determination of fusion through its core. The combination of the wealth of data gathered on the PTC components (mechanical, surface typography, in vitro, and the initial in vivo study) and the increased structural integrity of the fusion mass when using a PTC interbody device in a large animal model, gives credence to the notion that the PTC interbody device could lead to a faster and more robust intervertebral fusion relative to a standard PEEK device in a clinical setting.

References

1. Smith GW, Robinson RA. The treatment of certain cervical-spine disorders by anterior removal of the intervertebral disc and interbody fusion. J Bone Joint Surg Am. 1958;40-A(3):607–24.
2. Briggs H, Milligan PR. Chip fusion of the low back following exploration of the spinal canal. J Bone Joint Surg Am. 1944;26(1):125–30.
3. Jaslow I. Intercorporal bone graft in spinal fusion after disc removal. Surg Gynecol Obstet. 1946;82:215–8.
4. Cloward RB. The treatment of ruptured lumbar intervertebral discs by vertebral body fusion: I. Indications, operative technique, after care. J Neurosurg. 1953;10(2):154–68.
5. Anderson DG, Albert TJ. Bone grafting, implants, and plating options for anterior cervical fusions. Orthop Clin North Am. 2002;33(2):317–28.
6. Floyd T, Ohnmeiss D. A meta-analysis of autograft versus allograft in anterior cervical fusion. Eur Spine J. 2000;9(5):398–403.
7. Lemcke J, Al-Zain F, Meier U, Suess O. Polyetheretherketone (PEEK) spacers for anterior cervical fusion: A retrospective comparative effectiveness clinical trial. Open Orthop J. 2011;5:348–53.
8. Lofgren H, Engquist M, Hoffmann P, Sigstedt B, Vavruch L. Clinical and radiological evaluation of Trabecular Metal and the Smith-Robinson technique in anterior cervical fusion for degenerative disease: a prospective, randomized, controlled study with 2-year follow-up. European spine journal: official publication of the European Spine Society, the European

Spinal Deformity Society, and the European Section of the Cervical Spine Research. Society. 2010;19(3):464–73.

9. Samartzis D, Shen FH, Goldberg EJ, An HS. Is autograft the gold standard in achieving radiographic fusion in one-level anterior cervical discectomy and fusion with rigid anterior plate fixation? Spine. 2005;30(15):1756–61.

10. Silber JS, Anderson DG, Daffner SD, Brislin BT, Leland JM, Hilibrand AS, et al. Donor site morbidity after anterior iliac crest bone harvest for single-level anterior cervical discectomy and fusion. Spine. 2003;28(2):134–9.

11. Samartzis D, Shen FH, Matthews DK, Yoon ST, Goldberg EJ, An HS. Comparison of allograft to autograft in multilevel anterior cervical discectomy and fusion with rigid plate fixation. Spine J. 2003;3(6):451–9.

12. Cho DY, Liau WR, Lee WY, Liu JT, Chiu CL, Sheu PC. Preliminary experience using a polyetheretherketone (PEEK) cage in the treatment of cervical disc disease. Neurosurgery. 2002;51(6):1343–9. discussion 9–50.

13. Rousseau M-A, Lazennec J-Y, Saillant G. Circumferential arthrodesis using PEEK cages at the lumbar spine. Clin Spine Surg. 2007;20(4):278–81.

14. Zhou J, Xia Q, Dong J, Li X, Zhou X, Fang T, et al. Comparison of stand-alone polyetheretherketone cages and iliac crest autografts for the treatment of cervical degenerative disc diseases. Acta Neurochir. 2011;153(1):115–22.

15. Chou YC, Chen DC, Hsieh WA, Chen WF, Yen PS, Harnod T, et al. Efficacy of anterior cervical fusion: comparison of titanium cages, polyetheretherketone (PEEK) cages and autogenous bone grafts. J Clin Neurosci. 2008;15(11):1240–5.

16. Lin B, Yu H, Chen Z, Huang Z, Zhang W. Comparison of the PEEK cage and an autologous cage made from the lumbar spinous process and laminae in posterior lumbar interbody fusion. BMC Musculoskelet Disord. 2016;17(1):374.

17. Kurtz SM, Devine JN. PEEK biomaterials in trauma, orthopedic, and spinal implants. Biomaterials. 2007;28(32):4845–69.

18. Abdullah MR, Goharian A, Abdul Kadir MR, Wahit MU. Biomechanical and bioactivity concepts of polyetheretherketone composites for use in orthopedic implants-a review. J Biomed Mater Res A. 2015;103(11):3689–702.

19. Ma R, Tang T. Current strategies to improve the bioactivity of PEEK. Int J Mol Sci. 2014;15(4):5426–45.

20. Ratner BD. Biomaterials science: an introduction to materials in medicine. 2nd ed. Amsterdam: Elsevier/Academic Press; 2004. p. 851.

21. Cohen RA. porous tantalum trabecular metal: basic science. Am J Orthop. 2002;31(4):216–7.

22. Anselme K, Ponche A, Bigerelle M. Relative influence of surface topography and surface chemistry on cell response to bone implant materials. Part 2: biological aspects. Proc Inst Mech Eng H J Eng Med. 2010;224(12):1487–507.

23. Albrektsson T, Johansson C. Osteoinduction, osteoconduction and osseointegration. European spine journal: official publication of the European Spine Society, the European Spinal Deformity Society, and the European Section of the Cervical Spine Research. Society. 2001;10(Suppl 2):S96–101.

24. Miron RJ, Zhang YF. Osteoinduction: a review of old concepts with new standards. J Dent Res. 2012;91(8):736–44.

25. Clarkin CE, Gerstenfeld LC. VEGF and bone cell signalling: an essential vessel for communication? Cell Biochem Funct. 2013;31(1):1–11.

26. Jayakumar P, Di Silvio L. Osteoblasts in bone tissue engineering. Proc Inst Mech Eng H J Eng Med. 2010;224(12):1415–40.

27. Ochsner PE. Osteointegration of orthopaedic devices. Semin Immunopathol. 2011;33(3):245–56.

28. Ponche A, Bigerelle M, Anselme K. Relative influence of surface topography and surface chemistry on cell response to bone implant materials. Part 1: physico-chemical effects. Proc Inst Mech Eng H J Eng Med. 2010;224(12):1471–86.

29. Olivares-Navarrete R, Gittens RA, Schneider JM, Hyzy SL, Haithcock DA, Ullrich PF, et al. Osteoblasts exhibit a more differentiated phenotype and increased bone morphogenetic protein production on titanium alloy substrates than on poly-ether-ether-ketone. Spine J. 2012;12(3):265–72.

30. Karageorgiou V, Kaplan D. Porosity of 3D biomaterial scaffolds and osteogenesis. Biomaterials. 2005;26(27):5474–91.

31. Sevilla P, Aparicio C, Planell JA, Gil FJ. Comparison of the mechanical properties between tantalum and nickel–titanium foams implant materials for bone ingrowth applications. J Alloys Compunds. 2007;439(1–2):67–73.

32. Levi AD, Choi WG, Keller PJ, Heiserman JE, Sonntag VK, Dickman CA. The radiographic and imaging characteristics of porous tantalum implants within the human cervical spine. Spine. 1998;23(11):1245–50. Discussion 51.

33. Rudisch A, Kremser C, Peer S, Kathrein A, Judmaier W, Daniaux H. Metallic artifacts in magnetic resonance imaging of patients with spinal fusion. A comparison of implant materials and imaging sequences. Spine. 1998;23(6):692–9.

34. Wang JC, Yu WD, Sandhu HS, Tam V, Delamarter RB. A comparison of magnetic resonance and computed tomographic image quality after the implantation of tantalum and titanium spinal instrumentation. Spine. 1998;23(15):1684–8.

35. Nuss KM, von Rechenberg B. Biocompatibility issues with modern implants in bone - a review for clinical orthopedics. Open Orthop J. 2008;2:66–78.

36. Shapiro IM, Hickok NJ, Parvizi J, Stewart S, Schaer TP. Molecular engineering of an orthopaedic implant: from bench to bedside. Eur Cell Mater. 2012;23:362–70.

37. Baril E, Lefebvre LP, Hacking SA. Direct visualization and quantification of bone growth into porous titanium implants using micro computed tomography. J Mater Sci Mater Med. 2011;22(5):1321–32.

38. Jasty M, Bragdon C, Burke D, O'Connor D, Lowenstein J, Harris WH. In vivo skeletal responses to porous-surfaced implants subjected to small induced motions. J Bone Joint Surg Am. 1997;79(5):707–14.

39. de Vasconcellos LMR, dOM V, Graca MLA, dVLG O, Carvalho YR, Cairo CAA. Porous titanium scaffolds produced by powder metallurgy for biomedical applications. Mater Res. 2008;11(3):275–80.

40. Murr LE, Quinones SA, Gaytan SM, Lopez MI, Rodela A, Martinez EY, et al. Microstructure and mechanical behavior of Ti-6Al-4V produced by rapid-layer manufacturing, for biomedical applications. J Mech Behav Biomed Mater. 2009;2(1):20–32.

41. Biemond JE, Hannink G, Jurrius AM, Verdonschot N, Buma P. In vivo assessment of bone ingrowth potential of three-dimensional e-beam produced implant surfaces and the effect of additional treatment by acid etching and hydroxyapatite coating. J Biomater Appl. 2012;26(7):861–75.

42. ASTM F2924 - Standard Specification for Additive Manufacturing Titanium-6 Aluminum-4 Vanadium with Powder Bed Fusion. 2014.

43. ASTM F2077. Test Methods For Intervertebral Body Fusion Devices. 2011.

44. Chuang YM, Jack KS, Cheng HH, Whittaker AK, Blakey I. Using directed self assembly of block copolymer nanostructures to modulate nanoscale surface roughness: Towards a novel lithographic process. Adv Funct Mater. 2013;23(2):173–83.

45. Hu X, Park S-H, Gil ES, Xia X-X, Weiss AS, Kaplan DL. The influence of elasticity and surface roughness on myogenic and osteogenic-differentiation of cells on silk-elastin biomaterials. Biomaterials. 2011;32(34):8979–89.

46. Gittens RA, Olivares-Navarrete R, Schwartz Z, Boyan BD. Implant osseointegration and the role of microroughness and nanostructures: lessons for spine implants. Acta Biomater. 2014;10(8):3363–71.

47. Fang S, Jiang J. Micro-and Nano-scale surface topographic characterization of a novel PEEK Titanium Structural Composite. Society for Biomaterials annual meeting; April 6–10, 2017; Minneapolis, Minneapolis, USA.

48. Waldorff EI, Raines AL, Patel N, Ryaby JT. An In-vitro evaluation of bone formation response to the PEEK Titanium Composite (PTC) device components. American Association of Neurological Surgeons (AANS) Annual Scientific Meeting; Electronic poster #1383, April 5–9, 2014; San Francisco, California, USA.

49. Saino E, Grandi S, Quartarone E, Maliardi V, Galli D, Bloise N, et al. In vitro calcified matrix deposition by human osteoblasts onto a zinc-containing bioactive glass. Eur Cell Mater. 2011; 21:59–72.

50. Holtorf HL, Datta N, Jansen JA, Mikos AG. Scaffold mesh size affects the osteoblastic differentiation of seeded marrow stromal cells cultured in a flow perfusion bioreactor. J Biomed Mater Res A. 2005;74((2):171–80.

51. Waldorff EI, Easley J, Puttlitz C, Seim H, Zhang N, Ryaby JT, et al. Evaluation of a novel PEEK Titanium Composite (PTC) interbody cage in an ovine lumbar interbody fusion. Orthopaedic Research Society (ORS); Spine Implants, Paper #: 0088, March 19–22, 2017; San Diego, California, USA.

52. Waldorff EI, Goldberg E, Ryaby JT. An In-vivo evaluation of bone adaptation to the PEEK Titanium Composite (PTC) device endplates. American Association of Neurological Surgeons (AANS) Annual Scientific Meeting; Electronic poster #1384, April 5–9, 2014; San Francisco, California, USA.

53. US Food Administration FDA. Guidance for industry and FDA staff: General considerations for animal studies for cardiovascular devices. Washington, DC: US Department of Health and Human Services; 2010.

54. Institute of Laboratory Animal Research. Guide for the care and use of laboratory animals. 8th ed. Washington, DC: Institute of Laboratory Animal Research; 2011.

55. Anderson HC, Hsu HHT, Raval P, Reynold PR, Gurley DJ, Aguilera MX, et al. Bone-inducing agent in Saos-2 cell extracts and secretions. Cells Mater. 1998;8:89–98.

56. Manolagas SC. Birth and death of bone cells: basic regulatory mechanisms and implications for the pathogenesis and treatment of osteoporosis. Endocr Rev. 2000;21(2):115–37.

57. Owen TA, Aronow M, Shalhoub V, Barone LM, Wilming L, Tassinari MS, et al. Progressive development of the rat osteoblast phenotype in vitro: reciprocal relationships in expression of genes associated with osteoblast proliferation and differentiation during formation of the bone extracellular matrix. J Cell Physiol. 1990;143(3):420–30.

58. Quarles LD, Yohay DA, Lever LW, Caton R, Wenstrup RJ. Distinct proliferative and differentiated stages of murine MC3T3-E1 cells in culture: an in vitro model of osteoblast development. J Bone Miner Res. 1992;7(6):683–92.

59. van Dijk S, D'Errico JA, Somerman MJ, Farach-Carson MC, Butler WT. Evidence that a non-RGD domain in rat osteopontin is involved in cell attachment. J Bone Miner Res. 1993;8(12):1499–506.

60. Denhardt DT, Guo X. Osteopontin: a protein with diverse functions. FASEB J. 1993;7(15): 1475–82.

61. Aubin JE, Liu F. The osteobalst lineage. In: Bilezkian JP, Raisz LG, Rodan GA, editors. Principles of Bone Biology. San Diego, CA: Academic Press; 1996. p. 51–67.

62. Postiglione L, Di Domenico G, Ramaglia L, Montagnani S, Salzano S, Di Meglio F, et al. Behavior of SaOS-2 cells cultured on different titanium surfaces. J Dent Res. 2003;82(9):692–6.

63. Shapira L, Klinger A, Tadir A, Wilensky A, Halabi A. Effect of a niobium-containing titanium alloy on osteoblast behavior in culture. Clin Oral Implants Res. 2009;20(6):578–82.

64. Zernik J, Twarog K, Upholt WB. Regulation of ALP and alpha 2(I) procollagen synthesis during early intramembranous bone formation in the rat mandible. Differentiation. 1990; 44(3):207–15.

65. Gerstenfeld LC, Chipman SD, Glowacki J, Lian JB. Expression of differentiated function by mineralizing cultures of chicken osteoblasts. Dev Biol. 1987;122(1):49–60.

66. Czekanska EM, Stoddart MJ, Richards RG, Hayes JS. In search of an osteoblast cell model for in vitro research. Eur Cell Mater. 2012;24:1–17.

67. Cheng A, Humayun A, Cohen DJ, Boyan BD, Schwartz Z. Additively manufactured 3D porous Ti-6Al-4V constructs mimic trabecular bone structure and regulate osteoblast proliferation, differentiation and local factor production in a porosity and surface roughness dependent manner. Biofabrication. 2014;6(4):045007.
68. Li X, Luo Y, Wang C, Zhang W, Li Y. Fabrication and in vivo evaluation of Ti6Al4V implants with controlled porous structure and complex shape. Front Mech Eng. 2012;7(1):66–71.
69. Li JP, Habibovic P, van den Doel M, Wilson CE, de Wijn JR, van Blitterswijk CA, et al. Bone ingrowth in porous titanium implants produced by 3D fiber deposition. Biomaterials. 2007;28(18):2810–20.
70. An YH, Friedman RJ. Animal models in orthopaedic research. Boca Raton: CRC; 1999. p. 604.
71. Brentel AS, de Vasconcellos LM, Oliveira MV, Graca ML, de Vasconcellos LG, Cairo CA, et al. Histomorphometric analysis of pure titanium implants with porous surface versus rough surface. J Appl Oral Sci. 2006;14(3):213–8.
72. Suzuki K, Aoki K, Ohya K. Effects of surface roughness of titanium implants on bone remodeling activity of femur in rabbits. Bone. 1997;21(6):507–14.
73. Vasconcellos LM, Leite DO, Oliveira FN, Carvalho YR, Cairo CA. Evaluation of bone ingrowth into porous titanium implant: histomorphometric analysis in rabbits. Braz Oral Res. 2010;24(4):399–405.